Correlation effects on the nonmesonic weak decay of the Λ hyperon in nuclear matter

N. J. Robertson and W. H. Dickhoff*
Department of Physics, Washington University, St. Louis, Missouri 63130, USA
(Received 25 April 2005; published 31 August 2005)

The nonmesonic weak decay of a Λ hyperon is studied in nuclear matter. Special emphasis is placed on a consistent treatment of correlations introduced by the strong interaction on its weak counterpart. The latter is described by the exchange of mesons between the initial ΛN state and the final NN one. The weak decay is studied in terms of the weak self-energy, which allows a systematic evaluation of short-range and tensor correlation effects that are determined by a realistic hyperon-nucleon interaction. The admixture of ΣN components through the strong interaction is also included in the calculation of the Λ decay properties. Calculations for the ratio of the neutron-induced partial width to the corresponding proton-induced one, Γ_n/Γ_p, are discussed in connection with recent experimental results.

DOI: 10.1103/PhysRevC.72.024320 PACS number(s): 21.80.+a, 21.65.+f

I. INTRODUCTION

Hypernuclei continue to be studied widely, with early reviews going back to Refs. [1,2]. In view of the relevance of the properties of a strange particle in a nuclear system, the study of an embedded Λ hyperon has taken many forms. The binding properties of a Λ hyperon have been studied by several groups [3–6]. The general conclusion, confirmed by experiment, is that the Λ hyperon is bound in a potential well with a depth of about 30 MeV in heavier nuclei. Additional information is available from the Λ self-energy studied in Refs. [7,8]. Global properties of the Λ hyperon can be studied in nuclear matter (NM). Results of such calculations have also been reported by several groups [9–15]. The onset of hyperon formation in neutron stars [13,14,16] and the equation of state including hyperons have been studied in Refs. [17–21]. The stability of strange matter has been discussed in Refs. [22,23], and the properties of a neutron star, including strangeness, have been explored in Refs. [24,25].

As in the case of nucleon-nucleon (NN) interactions, typical hyperon-nucleon (YN) interactions [26–31] incorporate substantial repulsion at short relative distances. The consequences of such realistic interactions on the single-particle (sp) properties of a Λ have recently been studied recently by use of the Green's function method [32]. The presence of a Λ hyperon in the nuclear environment automatically requires the consideration of its heavier sibling, the Σ hyperon, on account of their strong coupling, mediated by pion exchange, which is present in realistic interactions. When the coupled ΛN-ΣN equations are solved for the effective interaction (G matrix), it becomes possible to fully explore the Λ self-energy and spectral functions in the medium. The work of Ref. [32] demonstrates that such correlation effects on a Λ are weaker than for a nucleon but still reduce its production probability on top of the ground state by about 15% compared with the noninteracting case, whereas for a nucleon this reduction is about 30%. It is the purpose of the present work to explore the consequences of the study reported in Ref. [32] on the weak-decay properties of a Λ in NM.

The weak decay of Λ hypernuclei continues to provide an intriguing window on the properties of strangeness inside the nuclear environment. Several review articles are available that discuss this topic [33–36]. In free space the Λ decays primarily through the weak pionic modes [Fig. 1(a)],

$$\Lambda \rightarrow p + \pi^- + 38\,\text{MeV}\,(64\%), \tag{1}$$

$$\Lambda \rightarrow n + \pi^0 + 41\,\text{MeV}\,(36\%), \tag{2}$$

with a lifetime of

$$\tau_\Lambda = 2.63 \times 10^{-10}\,\text{s}, \tag{3}$$

which corresponds to a decay width of

$$\Gamma_\Lambda = 2.5 \times 10^{-12}\,\text{MeV}. \tag{4}$$

In the center of mass of the decaying Λ, the final-state particles have momenta of about 100 MeV/c. The presence of a nuclear medium forces fundamental changes in the Λ decay mode. If one imagines producing a Λ at rest in a Fermi gas of nucleons ($k_F = 270$ MeV/c), then the final-state nucleon in Fig. 1(a) is Pauli blocked, resulting in complete suppression of the mesonic decay mode. In a realistic nuclear medium, correlations among the nucleons "soften" the sharp momentum-distribution characteristic of a Fermi gas [37]. Although this might seem to indicate a significant easing of the Pauli restriction, energy- and momentum-conservation requirements for the decay still ensure that the mesonic decay width in heavy hypernuclei is well below the free width [38].

If interactions between the Λ and nucleons in the medium are considered, then a new two-body decay mode becomes possible, as illustrated in Fig. 1(b). The weak vertex is the same as in Fig. 1(a), but now the meson is subsequently absorbed by a nucleon from the medium, resulting in a net $YN \rightarrow NN$ transition. Because this nonmesonic mode involves a virtual meson exchange, the entire Λ-N mass difference of 176 MeV is made available for the kinetic energy of

*Electronic address: wimd@wuphys.wustl.edu; http://www.physics.wustl.edu/~wimd

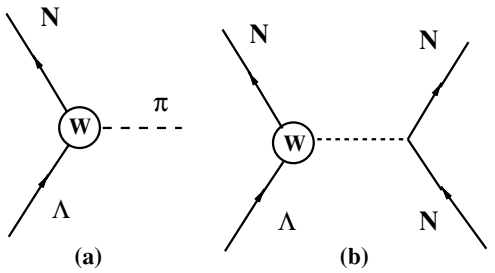

FIG. 1. Part (a) illustrates the mesonic decay and part (b) the nonmesonic decay of the Λ hyperon. The weak vertex is indicated by a circle containing a W.

the final-state particles. This translates into a momentum of about 400 MeV/c for the final-state nucleons, overcoming any Pauli blocking. Because the nonmesonic decay is catalyzed by a nucleon from the medium, the decay rate is expected to be proportional to the nuclear density. Conversely, the mesonic decay is suppressed at high nuclear densities, and it follows that the nonmesonic mode will dominate for sufficiently heavy hypernuclei. Experimentally, it is found that the nonmesonic mode dominates for all but the very lightest hypernuclei [34].

One can fruitfully perform general studies of this process by considering the weak nonmesonic decay in NM. Many theoretical calculations employ as a starting point the weak pion-exchange mechanism [39–42]. Both the weak and strong vertices of this interaction are constrained by experimental data. Less is known about other meson-exchange contributions but the work of Ref. [42] has often been employed to include such terms. The effect of form factors (FFs) and the treatment of short-range correlations (SRCs) have been incorporated in previous studies. Such treatments of SRCs typically involve the introduction of a correlation function in coordinate space, which suppresses the weak amplitude at short distances. Although such correlation functions have been related qualitatively to microscopic G-matrix calculations by use of realistic ΛN interactions, it appears that no detailed investigation of a consistent treatment of SRCs is available. In particular, the strong interaction between the Λ and a nucleon in the medium is capable of inducing tensor, i.e., nondiagonal, correlations, as well as (diagonal) SRCs into the relative wave function before the Λ decays [32]. These microscopically calculated effects of the strong interaction on the ΛN relative wave function provide the appropriate tools for studying the nonmesonic decay properties. The strong coupling to the ΣN channel generates additional relative wave-function components that also require a treatment at the same level as the ΛN ones [43,44].

The paper starts in Sec. II with the introduction of the relevant formalism for the determination of the lowest-order weak self-energy of the Λ in NM. The weak meson-exchange potential employed in this work is presented in Sec. III. Results without the inclusion of correlations are discussed in Sec. IV to establish contact with other calculations in the literature. The effects of a consistent treatment of SRCs on the nonmesonic weak decay of the Λ are then documented in Sec. V. This

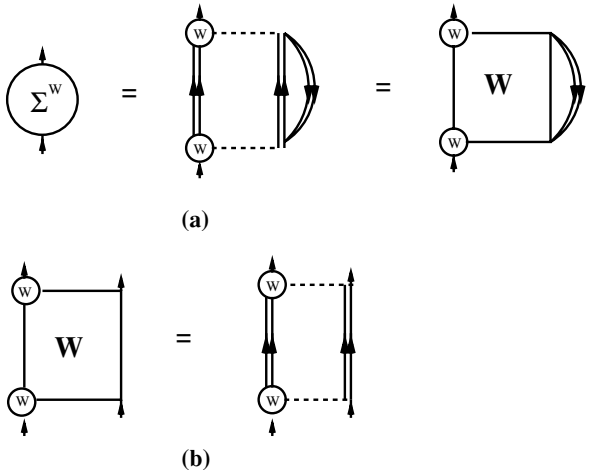

FIG. 2. Part (a) illustrates the lowest-order self-energy diagram for nonmesonic Λ decay. External lines represent Λ particles and internal lines represent nucleons, which should, in principle, be dressed by the medium (double lines). In part (b) the weak effective interaction, denoted by the square containing W, is approximated by the second-order contribution in the weak interaction. For strange meson exchange the weak and strong vertices must be switched. The W box can be generalized to include the effects of SRCs and tensor correlations induced by the strong interaction.

section also contains a discussion of the relevance of the present results for corresponding quantities in finite nuclei. This includes a discussion of the ratio of the neutron-induced partial width, $\Gamma_{\Lambda n\to nn}$, to the proton-induced one, $\Gamma_{\Lambda p\to np}$. This ratio is often denoted by Γ_n/Γ_p. Earlier experimental results in hypernuclei yielded a value of the order of 1 whereas theoretical results generated much smaller values for this quantity. Only recently smaller experimental values for this ratio have been obtained when nucleon-nucleon coincidence data were employed. Details related to wound integrals are relegated to the appendix.

II. SELF-ENERGY AND THE WEAK-DECAY WIDTH

The nonmesonic decay width may be expressed in terms of the second-order self-energy diagram [33] shown in Fig. 2(a):

$$\Gamma_\Lambda^{(\mathrm{nm})}(k) = -2\,\mathrm{Im}\Sigma_\Lambda^{(\mathrm{nm})}(k). \tag{5}$$

The self-energy is evaluated on-shell and averaged over the spin of the Λ:

$$\Sigma_\Lambda^{(\mathrm{nm})}(k) \equiv \frac{1}{2}\sum_\alpha \Sigma_\Lambda^{(\mathrm{nm})}(k\alpha;\varepsilon_\Lambda(k)), \tag{6}$$

where sp spin and isospin quantum numbers are denoted by

$$|\alpha\rangle \equiv |sm_s tm_t\rangle. \tag{7}$$

By use of standard Feynman diagram rules [45–47], the self-energy of Fig. 2(a) is given by

$$\Sigma_\Lambda^{(\mathrm{nm})}(k) = \frac{1}{2}\sum_{\alpha\beta}\int\frac{d\omega'}{2\pi i}\int\frac{d^3p}{2\pi^3} \times \langle\vec{k}\alpha;\vec{p}\beta|W(Q;\varepsilon_\Lambda(k)+\omega')|\vec{k}\alpha;\vec{p}\beta\rangle g_N(p;\omega'), \tag{8}$$

where the second-order weak-transition matrix [Fig. 2(b)] is defined by

$$\langle\vec{k}\alpha;\vec{p}\beta|W(Q;\Omega)|\vec{k}\alpha;\vec{p}\beta\rangle = -\frac{1}{2}\sum_{\mu\lambda}\int d^3q_1\int d^3q_2\langle\vec{k}\alpha;\vec{p}\beta|V^{(w)}|\vec{q}_1\mu;\vec{q}_2\lambda\rangle \times g_{NN}^{\mathrm{II}}(\vec{q}_1,\vec{q}_2;\Omega)\langle\vec{q}_1\mu;\vec{q}_2\lambda|V^{(w)}|\vec{k}\alpha;\vec{p}\beta\rangle, \tag{9}$$

including the two-nucleon propagator g_{NN}^{II} further specified in Sec. II A. The nucleon hole propagator is taken to have the form appropriate for a noninteracting particle:

$$g_N(p;\omega') = \frac{\Theta(k_F-p)}{\omega'-\varepsilon_N(p)-i\eta}. \tag{10}$$

Changing to total spin and isospin

$$\vec{S} = \vec{s}_\Lambda + \vec{s}_N, \tag{11}$$

$$\vec{T} = \vec{t}_\Lambda + \vec{t}_N, \tag{12}$$

and to total and relative momentum,

$$\vec{Q} \equiv \vec{k} + \vec{p}, \tag{13}$$

$$\vec{q} \equiv \left(\frac{\mu_\Lambda}{m_N}\right)\vec{p} - \left(\frac{\mu_\Lambda}{m_\Lambda}\right)\vec{k}, \tag{14}$$

leads to

$$\frac{1}{2}\sum_{\alpha\beta}\langle\vec{k}\alpha;\vec{p}\beta|W(Q;\Omega)|\vec{k}\alpha;\vec{p}\beta\rangle = \frac{1}{4}\sum_{ST}\sum_{M_S M_S'}(2T+1)\langle\vec{q}SM_ST|W(Q;\Omega)|\vec{q}SM_S'T\rangle. \tag{15}$$

Making a change in the integration variable from $\vec{p}$ to $\vec{Q}$, performing the integration over the nucleon hole energy, and expanding in a partial-wave basis transform Eq. (8) into

$$\Sigma_\Lambda^{(\mathrm{nm})}(k) = \frac{1}{4}\sum_{JLT}(2J+1)(2T+1) \times \int dQ\,Q^2\int_{\xi_Q^{\min}}^1\frac{d\xi_Q}{2}\langle qJ(LS)T|W \times [Q;\varepsilon_\Lambda(k)+\varepsilon_N(p)]|qJ(LS)T\rangle, \tag{16}$$

where

$$q = q(k,Q,\xi_Q), \tag{17}$$

$$p = p(k,Q,\xi_Q), \tag{18}$$

ξ_Q is the cosine of the angle between $\vec{Q}$ and $\vec{k}$, and

$$\langle qJ(LS)T|W(Q;\Omega)|qJ(LS)T\rangle = -\frac{1}{2}\sum_{L'}\int d^3q'|\langle qJ(LS)T|V^w|q'J(L'S')T\rangle|^2 \times \bar{g}_{NN}^{II}(q',Q;\Omega). \tag{19}$$

Equations (5), (16), and (19) yield the following expression for the decay width:

$$\Gamma_\Lambda^{(\mathrm{nm})}(k) = -\frac{1}{8}\sum_{JLL'T}(2J+1)(2T+1)\int dQ\,Q^2 \times\int_{\xi_Q^{\min}}^1\frac{d\xi_Q}{2}\int d^3q'|\langle qJ(LS)T|V^w|q'J(L'S')T\rangle|^2 \times \mathrm{Im}\,\bar{g}_{NN}^{\mathrm{II}}(q',Q;\Omega). \tag{20}$$

A. Approximate expression for the weak-decay width

To facilitate comparison with other work and simplify the numerical calculation, Eq. (20) is further modified in this section. The two-particle energy, $\Omega \equiv \varepsilon_\Lambda(k)+\varepsilon_N(p)$, is dependent on the integration variables through the nucleon hole momentum, as indicated in Eq. (18). The nucleon hole propagator in Eq. (10) contains a Pauli function that restricts the nucleon momentum to a range below k_F. The two-nucleon propagator in Eq. (19) may be evaluated at a single energy if an average value of the nucleon momentum,

$$\bar{p} \equiv \frac{3k_F}{5}, \tag{21}$$

is used as an approximation.

When the noninteracting particle approximation is used for the intermediate nucleons, the angle-averaged two-particle propagator is

$$\bar{g}_{NN}^{\mathrm{II}}(q,Q;\Omega) = \frac{-\Theta_{NN}(q,Q;k_F)}{\Omega-\bar{\varepsilon}_{NN}(q,Q)+i\eta}, \tag{22}$$

where Θ represents the angle-averaged version incorporating the Pauli principle for the two-nucleon state (see, e.g., Ref. [48]). A similar angle averaging is applied to the two-particle energy in the denominator of Eq. (22). The imaginary part is then given by

$$\mathrm{Im}\bar{g}_{NN}^{\mathrm{II}}(q,Q;\Omega) = \pi\delta(\Omega-\bar{\varepsilon}_{NN}(q,Q)) = \pi\left|\frac{\partial\bar{\varepsilon}_{NN}}{\partial q}\right|_{q=q_0}^{-1}\delta(q-q_0), \tag{23}$$

where q_0 is defined by

$$\bar{\varepsilon}_{NN}(q_0,Q) \equiv \Omega + (M_\Lambda - M_N). \tag{24}$$

The two-particle energy Ω, as determined from the initial ΛN state by use of the average momentum $\bar{p}$ for a nucleon hole and $k=0$ for the Λ, is

$$\Omega = \varepsilon_\Lambda(k)+\varepsilon_N(\bar{p}) \approx -80\,\mathrm{MeV}. \tag{25}$$

With this value of the two-particle energy, the angle-averaged value of the final-state two-nucleon energy is

$$\bar{\varepsilon}_{NN}(q_0,Q) = 2\varepsilon_N(\bar{q}_N) \approx -80 + (1116-939)\,\mathrm{MeV}, \quad \varepsilon_N(\bar{q}_N) \approx 52\,\mathrm{MeV}, \tag{26}$$

which yields a value of the relative momentum, $\bar{q}_N \approx 420$ MeV/c.

For a Λ at rest, the total momentum is just $Q = \bar{p} \approx 160$ MeV/c, which is sufficiently small compared with $\bar{q}_N$

that $\bar{q}_N(q_0; Q) \approx q_0$ to a good approximation. The derivative of the two-nucleon energy in Eq. (23) may be evaluated as

$$\frac{\partial \bar{\varepsilon}_{NN}(q_0, Q)}{\partial q} \approx 2\frac{\partial \varepsilon_N(q_0)}{\partial q} \equiv 2\frac{q_0}{M_N^*}, \tag{27}$$

where a nucleon effective mass M_N^* has been introduced. The nucleon energy spectrum is

$$\varepsilon_N(q) \equiv t_N(q) + U_N(q), \tag{28}$$

where a Woods-Saxon parametrization is used to fit a numerically determined nucleon sp potential. The ratio M_N/M_N^* is approximately 1.37 for $q_0 = 420$ MeV/c and goes to unity as q_0 becomes large enough that the potential term in Eq. (28) can be neglected [32].

The resulting expression for the imaginary part of the two-nucleon propagator is

$$\mathrm{Im}\, \bar{g}_{NN}^{\mathrm{II}}(q, \bar{Q}; \bar{\Omega}) = \frac{i\pi M_N^*}{2q_0}\delta(q - q_0), \tag{29}$$

and the W matrix is

$$\langle q J(LS)T|W(\bar{Q}; \bar{\Omega})|q J(LS)T\rangle = -\frac{\pi M_N^* q_0}{4}\sum_{L'}|\langle q J(LS)T|V^w|q_0 J(L'S')T\rangle|^2. \tag{30}$$

The remaining dependence on the integration variables Q and ξ_Q can be eliminated by taking an average value of the relative momentum $q(Q, \xi_Q; k)$ in the initial ΛN state. The imaginary part of the on-shell self-energy from Eq. (16) is

$$\mathrm{Im}\, \bar{\Sigma}_\Lambda^{(\mathrm{nm})}(k) = \frac{1}{4}\sum_{JLT}(2J+1)(2T+1)\frac{k_F^3}{3}\left[-\frac{\pi M_N^* q_0}{4} \times \sum_{L'}|\langle \bar{q} J(LS)T|V^w|q_0 J(L'S')T\rangle|^2\right], \tag{31}$$

with $\bar{q} \approx 70$ MeV/c. This yields a simple approximation for the nonmesonic decay width

$$\bar{\Gamma}_\Lambda^{(\mathrm{nm})}(0) = \frac{3\pi^3}{16}(q_0 M_N^* \rho)\sum_{JLL'T}(2J+1)(2T+1) \times |\langle \bar{q} J(LS)T|V^w|q_0 J(L'S')T\rangle|^2, \tag{32}$$

where ρ denotes the nuclear density. Calculation of the weak-decay width is now reduced to evaluating a few matrix elements of the $\Lambda N \to NN$ transition potential. This approach is similar to that used in Ref. [40]. Although the use of Eq. (32) is not strictly necessary, it provides a sufficiently accurate representation of the more general result of Eq. (20) and makes the comparison with earlier work more straightforward. Furthermore, the expression of the width in this form facilitates the presentation of the inclusion of the influence of the coupling to the ΣN on the decay properties (see Sec. V B).

III. THE WEAK MESON-EXCHANGE POTENTIAL

A weak meson-exchange interaction may be constructed formally in much the same way as the strong Nijmegen and Jülich potentials [26–31]. Parameters of the strong interaction are determined by fits to YN scattering data (and NN scattering data through the use of flavor symmetries). This procedure determines coupling constants for the strong NNm vertices that may be carried over directly to the weak interaction. The only experimentally accessible quantities that can be readily related to needed weak-coupling constants are hyperon decay amplitudes and these provide information only for the $YN\pi$ vertices. The exchange of heavier mesons occurs only as a virtual process, and weak coupling constants must be derived in the context of some theoretical model.

TABLE I. Coupling constants in units of $G_F m_\pi^2 = 2.21 \times 10^{-7}$ are taken from Table XII-5 in Ref. [50], except the sign of the B values has been flipped to correspond with the Bjorken and Drell [51] sign convention for γ_5. Coupling constants are calculated from data in Ref. [52]. The latest experimentally determined lifetimes, from which these coupling constants are generated, have errors less than 1% [53].

$Y \to N\pi$	A	B
$\Lambda \to p\pi^-$	1.47	−10.00
$\Lambda \to n\pi^0$	−1.07	7.15
$\Sigma^+ \to p\pi^0$	−1.48	−12.04
$\Sigma^+ \to n\pi^+$	0.06	−19.10
$\Sigma^- \to n\pi^-$	1.93	0.65

Except where noted, $\Lambda N \to NN$ potential matrix elements are generated with a code provided by Parreño, Ramos, and Bennhold, based on their work as reported in Ref. [49]. Necessary $\Sigma N \to NN$ matrix elements are related to the $\Lambda N \to NN$ matrix elements as discussed in Sec. III B.

A. Weak-coupling constants from experimental decay amplitudes

The amplitude for the $Y \to N\pi$ decay may be written [50] as

$$M_{Y\to N\pi} = \bar{U}_N(A + B\gamma_5)\phi_\pi U_Y. \tag{33}$$

The hyperon and nucleon fields are represented by U_Y and U_N, respectively, and the pion field by ϕ_π. A and B are coupling constants for the parity-violating (PV) and parity-conserving (PC) amplitudes, respectively. The partial width for this decay is found to be [50]

$$\Gamma_{Y\to N\pi} = \frac{q(E_N + m_N)}{4\pi m_Y}\left[|A|^2 + \left(\frac{E_N - m_N}{E_N + m_N}\right)|B|^2\right], \tag{34}$$

with

$$E_N = \left(m_N^2 + q^2\right)^{1/2}. \tag{35}$$

The constants A and B are obtained from experimental partial decay rates (which determine only the magnitudes) and polarization measurements (required for determining the signs). These are listed in Table I.

Although isospin is not conserved in weak interactions, it is empirically observed to change only in a restricted manner. As an example, expression (2) is consistent with a purely $T = 1/2$ final state even though the nucleon and pion can in

principle also couple to $T = 3/2$. This empirical $\Delta T = 1/2$ rule is also observed in kaon and Σ hyperon decays [54]. Although the reason for this rule is not well understood, it may be incorporated in the weak-decay formalism to find relationships among the coupling constants of Table I, reducing the number of independent amplitudes from 10 to 6.

The $\Delta T = 1/2$ rule may be implemented by the association with each hyperon state $|Y\rangle$ of a corresponding "spurion" state [54]:

$$|\tilde{Y}\rangle \equiv \left|\tfrac{1}{2} - \tfrac{1}{2}\right\rangle \otimes |Y\rangle. \tag{36}$$

Coupling to the "spurious" $|\frac{1}{2} - \frac{1}{2}\rangle$ isospin state enforces a change of 1/2 in the total isospin while conserving charge. The resulting isospin structure of the Λ spurion is

$$|\tilde{\Lambda}\rangle \equiv \left|\tfrac{1}{2} - \tfrac{1}{2}\right\rangle \otimes |00\rangle = \left|\tfrac{1}{2} - \tfrac{1}{2}\right\rangle. \tag{37}$$

Note that the Λ spurion has the same quantum numbers as a neutron. The spurion field may be used in place of the hyperon field to construct an isospin-conserving weak vertex, effectively mimicking a $\Delta T = 1/2$ transition. The amplitude of Eq. (33), modified to make use of the isospin 1/2 spurion field, becomes

$$M_{\Lambda\to N\pi} = \bar{U}_N(A_\Lambda + B_\Lambda\gamma_5)\vec{\tau}\cdot\vec{\phi}_\pi U_{\tilde{\Lambda}}, \tag{38}$$

where the vertex operator is now explicitly an isoscalar and A_Λ and B_Λ are isospin-independent "reduced" couplings for Λ decay. Aside from inclusion of the PV amplitude on the same footing as the PC amplitude, Eq. (38) for the weak vertex is exactly the same form as is typically used for the strong $NN\pi$ vertex.

The isospin structure of the Σ spurion is constructed in analogy with Eq. (37) [55] and yields

$$\begin{aligned}
|\tilde{\Sigma}^+\rangle &= \sqrt{\frac{2}{3}}\left|\frac{1}{2}\quad\frac{1}{2}\right\rangle - \sqrt{\frac{1}{3}}\left|\frac{3}{2}\quad\frac{1}{2}\right\rangle,\\
|\tilde{\Sigma}^0\rangle &= -\sqrt{\frac{1}{3}}\left|\frac{1}{2}-\frac{1}{2}\right\rangle + \sqrt{\frac{2}{3}}\left|\frac{3}{2}-\frac{1}{2}\right\rangle,\\
|\tilde{\Sigma}^-\rangle &= \left|\frac{3}{2}-\frac{3}{2}\right\rangle.
\end{aligned} \tag{39}$$

Note that the Σ spurions are a combination of isospin 1/2 and 3/2 components. As an example, the $\tilde{\Sigma}^+$ has a $t = 1/2$ component with the same isospin as a proton and a $t = 3/2$ component with the isospin of a Δ^+ isobar. In light of this isospin structure, the weak isoscalar vertex appropriate for Σ decay contains two terms:

$$\begin{aligned}
M_{\Sigma\to N\pi} = {}& \bar{U}_N\left(A_\Sigma^{(1)} + B_\Sigma^{(1)}\gamma_5\right)\vec{\tau}\cdot\vec{\phi}_\pi U_{\tilde{\Sigma}}\\
&+ \bar{U}_N\left(A_\Sigma^{(3)} + B_\Sigma^{(3)}\gamma_5\right)\vec{T}\cdot\vec{\phi}_\pi U_{\tilde{\Sigma}}.
\end{aligned} \tag{40}$$

The first term has the same form as Eq. (38) and accounts for decay from the isospin 1/2 component of the Σ spurion. The second term involves the isospin transition operator T, in place of τ, and accounts for decay from the isospin 3/2 component of the Σ spurion. The $\vec{T}\cdot\vec{\phi}$ operator is the form that is also used for a $\Delta N\pi$ vertex [56].

TABLE II. Reduced coupling constants in units of $G_F m_\pi^2$ as determined from the Λ pionic decays.

Decay	A	B
$\Lambda \to p\pi^-$	1.04	−7.07
$\Lambda \to n\pi^0$	1.07	−7.15
Average	1.05	−7.11

The spurion formalism implements the $\Delta T = 1/2$ rule, but also results in a weak-decay amplitude with a compact isospin structure that describes the $YN\pi$ vertex with a minimal number of coupling constants. One may determine these six independent constants (A_Λ, $A_\Sigma^{(1)}$, etc.…) from the data in Table I by evaluating the isospin operator for the various decay modes. Amplitudes for the two Λ decay channels may be expressed in terms of an isospin factor times an isospin-independent "reduced" amplitude:

$$a(\Lambda \to N\pi) \equiv \langle\tilde{\Lambda}|\vec{\tau}\cdot\vec{\phi}|N\pi\rangle\tilde{a}(\Lambda \to N\pi). \tag{41}$$

Evaluating the isospin factor for each decay channel [55] leads to

$$a(\Lambda \to p\pi^-) = \sqrt{2}\tilde{a}(\Lambda \to N\pi), \tag{42}$$

$$a(\Lambda \to n\pi^0) = -\tilde{a}(\Lambda \to N\pi). \tag{43}$$

These relationships hold separately for the PV and PC amplitudes and allow the reduced coupling constants (Table II) to be found.

For Σ decay, the amplitude for a particular decay channel may be expressed in terms of reduced amplitudes for each of the two isospin components that comprise the Σ spurion:

$$\begin{aligned}
a(\Sigma \to N\pi) &\equiv a^{(1)}(\Sigma \to N\pi) + a^{(3)}(\Sigma \to N\pi)\\
&\equiv \langle\tilde{\Sigma}|\vec{\tau}\cdot\vec{\phi}|N\pi\rangle\tilde{a}^{(1)}(\Sigma \to N\pi)\\
&\quad + \langle\tilde{\Sigma}|\vec{T}\cdot\vec{\phi}|N\pi\rangle\tilde{a}^{(3)}(\Sigma \to N\pi),
\end{aligned} \tag{44}$$

where

$$|\tilde{\Sigma}\rangle = \alpha\left|\tfrac{1}{2}m_{\tilde{\Sigma}}\right\rangle + \beta\left|\tfrac{3}{2}m_{\tilde{\Sigma}}\right\rangle, \tag{45}$$

with constants α and β as given in Eq. (39). Evaluating the isospin factor for each decay channel [55] leads to

$$\begin{aligned}
a(\Sigma^+ \to p\pi^0) &= \sqrt{\frac{2}{3}}\tilde{a}^{(1/2)}(\Sigma \to N\pi)\\
&\quad - \frac{\sqrt{2}}{3}\tilde{a}^{(3/2)}(\Sigma \to N\pi),
\end{aligned} \tag{46}$$

$$\begin{aligned}
a(\Sigma^+ \to n\pi^+) &= \frac{2}{\sqrt{3}}\tilde{a}^{(1/2)}(\Sigma \to N\pi)\\
&\quad + \frac{1}{3}\tilde{a}^{(3/2)}(\Sigma \to N\pi),
\end{aligned} \tag{47}$$

$$\begin{aligned}
a(\Sigma^0 \to p\pi^-) &= -\sqrt{\frac{2}{3}}\tilde{a}^{(1/2)}(\Sigma \to N\pi)\\
&\quad + \frac{\sqrt{2}}{3}\tilde{a}^{(3/2)}(\Sigma \to N\pi),
\end{aligned} \tag{48}$$

TABLE III. Reduced coupling constants in units of $G_F m_\pi^2$ as determined from the Σ pionic decays.

First decay	Second decay	$A^{(1)}$	$A^{(3)}$	$B^{(1)}$	$B^{(3)}$
$\Sigma^+ \to p\pi^0$	$\Sigma^+ \to n\pi^+$	−0.57	1.52	−15.94	−1.47
$\Sigma^+ \to p\pi^0$	$\Sigma^- \to n\pi^-$	−0.70	1.36	−14.37	0.46
$\Sigma^+ \to n\pi^+$	$\Sigma^- \to n\pi^-$	−0.51	1.36	−16.73	0.46
Average		−0.59	1.41	−15.68	−0.18

$$a(\Sigma^0 \to n\pi^0) = \frac{1}{\sqrt{3}}\tilde{a}^{(1/2)}(\Sigma \to N\pi) + \frac{2}{3}\tilde{a}^{(3/2)}(\Sigma \to N\pi), \quad (49)$$

$$a(\Sigma^- \to n\pi^-) = \tilde{a}^{(3/2)}(\Sigma \to N\pi). \quad (50)$$

Constants from two decay modes are required for determining both $T = 1/2$ and $T = 3/2$ sets of reduced coupling constants. Only three of the five possible decay modes given in Eqs. (46)–(50) have entries in Table I. This is because the Σ^0 decays primarily through an electromagnetic mode that masks the weak mesonic decay. The three remaining decay channels represented by Eqs. (46), (47), and (50) still overdetermine the desired couplings. Determining couplings from each pair of decay channels leads to the results of Table III. Note that there is more variation among the reduced coupling values for the Σ in Table III than for the Λ in Table II. This suggests that the $\Delta T = 1/2$ rule is not as well satisfied for Σ decays.

B. Isospin operators in the baryon-baryon basis

The two-baryon state composed of a Λ spurion, $|\frac{1}{2}-\frac{1}{2}\rangle$, and a nucleon, $|\frac{1}{2},\pm\frac{1}{2}\rangle$, can couple to total isospin 1 or 0:

$$|\tilde{\Lambda}N\rangle = \left|\frac{1}{2}-\frac{1}{2}\right\rangle \otimes \left|\frac{1}{2}m_N\right\rangle = \delta_{m_N}\frac{1}{2}\left\{\frac{1}{\sqrt{2}}[|10\rangle - |00\rangle]\right\} + \delta_{m_N-\frac{1}{2}}|1{-}1\rangle. \quad (51)$$

If the $|\tilde{\Lambda}N\rangle$ state now undergoes a strong transition to the $|\tilde{\Sigma}N\rangle$ state, how much of the $|\tilde{\Sigma}N\rangle = |1m\rangle$ state is $|(\frac{3}{2}\frac{1}{2})1m\rangle$ and how much is $|(\frac{1}{2}\frac{1}{2})1m\rangle$? Each of these states decays differently, so the decomposition is important. This apparent ambiguity arises because the strong interaction used in Ref. [29] (denoted as NSC89 from now on) does not treat the hyperons as spurions. For purposes of the strong interaction, the isospin of the ΛN state is

$$|\Lambda N\rangle = |00\rangle \otimes \left|\tfrac{1}{2}m\right\rangle = \left|\tfrac{1}{2}m\right\rangle, \quad (52)$$

and couples unambiguously to a ΣN state with the same isospin,

$$|\Sigma N\rangle = \left|\tfrac{1}{2}m\right\rangle. \quad (53)$$

This state can be decomposed into $|1m_\Sigma\rangle \otimes |\frac{1}{2}m_N\rangle$ product states. Now the Σ spurion can be introduced,

$$|1m_\Sigma\rangle \to \left|\tfrac{1}{2}-\tfrac{1}{2}\right\rangle \otimes |1m_\Sigma\rangle, \quad (54)$$

and coupled to the nucleon. This completes the $|\Sigma N\rangle \to |\tilde{\Sigma}N\rangle$ transformation in an unambiguous manner, and paves the way for calculation of the necessary $\tilde{Y}N \to NN$ weak-transition matrix elements. The final result is

$$\begin{aligned}|\Sigma N\rangle = \left|\frac{1}{2}m\right\rangle &\to |\tilde{\Sigma}N\rangle \\ &= \delta_{m\frac{1}{2}}\left\{\frac{2}{3}\left|\left(\frac{3}{2}\quad\frac{1}{2}\right)10\right\rangle - \frac{\sqrt{2}}{6}\left|\left(\frac{1}{2}\quad\frac{1}{2}\right)10\right\rangle \right. \\ &\quad \left. - \frac{1}{\sqrt{2}}\left|\left(\frac{1}{2}\quad\frac{1}{2}\right)10\right\rangle\right\} + \delta_{m-\frac{1}{2}}\left\{\frac{\sqrt{8}}{3}\left|\left(\frac{3}{2}\quad\frac{1}{2}\right)1-1\right\rangle \right. \\ &\quad \left. - \frac{1}{3}\left|\left(\frac{1}{2}\quad\frac{1}{2}\right)1-1\right\rangle\right\}. \end{aligned} \quad (55)$$

The details can be found in Ref. [55].

One may formally rewrite Eq. (55) in the same form as Eq. (51) for the $|\tilde{\Lambda}N\rangle$ state,

$$|\tilde{\Sigma}N\rangle = \delta_{m\frac{1}{2}}\left\{\frac{1}{\sqrt{2}}[|10\rangle - |00\rangle]\right\} + \delta_{m-\frac{1}{2}}|1{-}1\rangle, \quad (56)$$

by defining

$$|1m\rangle \equiv \sqrt{\frac{8}{9}}\left|\left(\frac{3}{2}\quad\frac{1}{2}\right)1m\right\rangle - \sqrt{\frac{1}{9}}\left|\left(\frac{1}{2}\quad\frac{1}{2}\right)1m\right\rangle, \quad (57)$$

$$|00\rangle \equiv \left|\left(\frac{1}{2}\quad\frac{1}{2}\right)00\right\rangle. \quad (58)$$

The transition potential for weak decay by means of virtual pion exchange is given by [50]

$$V_\pi(\vec{q}) = -G_F m_\pi^2 \frac{g_{NN\pi}}{2M_N}\left(A + \frac{B}{2\bar{M}_Y}\vec{\sigma}_1\cdot\vec{q}\right) \times \frac{\vec{\sigma}_2\cdot\vec{q}}{q^2+\mu^2}\hat{T}_{12}, \quad (59)$$

where

$$\bar{M}_Y \equiv \frac{M_N + M_Y}{2} \quad (60)$$

and

$$\hat{T}_{12} = \begin{cases}\vec{\tau}_1\cdot\vec{\tau}_2 & t = 1/2 \\ \vec{T}_1\cdot\vec{\tau}_2 & t = 3/2.\end{cases} \quad (61)$$

For the isospin transition operator $\hat{T}$ used in this work, the matrix elements of $\hat{T}_{12}$ on the two-baryon basis are determined to be

$$\left\langle\left(\frac{1}{2}\quad\frac{1}{2}\right)0m\left|\vec{\tau}_1\cdot\vec{\tau}_2\right|\left(\frac{1}{2}\quad\frac{1}{2}\right)0m\right\rangle = -3, \quad (62)$$

$$\left\langle\left(\frac{1}{2}\quad\frac{1}{2}\right)1m\left|\vec{\tau}_1\cdot\vec{\tau}_2\right|\left(\frac{1}{2}\quad\frac{1}{2}\right)1m\right\rangle = 1, \quad (63)$$

$$\left\langle\left(\frac{1}{2}\quad\frac{1}{2}\right)1m\left|\vec{T}_1\cdot\vec{\tau}_2\right|\left(\frac{3}{2}\quad\frac{1}{2}\right)1m\right\rangle = \frac{-4}{\sqrt{3}}. \quad (64)$$

These expressions, together with Eqs. (57)–(59) relate the $\Sigma N \to NN$ matrix elements to those for $\Lambda N \to NN$:

TABLE IV. Ratio of the weak matrix elements $V_{\Sigma N\to NN}$ to $V_{\Lambda N\to NN}$ for meson exchanges for which coupling constants are available. The ratio is different for the spin-independent and spin-dependent parts of the central potential, but this affects only the PC part of the K^* meson.

	π		K	K^*	
	$T=0$	$T=1$		Spin-dependent	Spin-independent
PC	2.12	−0.76	−0.29	−0.16	0.58
PV	−0.56	−2.74	−0.30	−0.16	

$$T=1:\frac{\langle\tilde{\Sigma}N|V_{\rm PV}|NN\rangle}{\langle\tilde{\Lambda}N|V_{\rm PV}|NN\rangle}=\left[\sqrt{\frac{8}{9}}\frac{A_\Sigma^{(3)}\langle T=1|\vec{T}_1\cdot\vec{\tau}_2|T=1\rangle}{A_\Lambda\langle T=1|\vec{\tau}_1\cdot\vec{\tau}_2|T=1\rangle}-\sqrt{\frac{1}{9}}\frac{A_\Sigma^{(1)}}{A_\Lambda}\right]=[-2.92+0.19]=-2.74, \tag{65}$$

$$\frac{\langle\tilde{\Sigma}N|V_{\rm PC}|NN\rangle}{\langle\tilde{\Lambda}N|V_{\rm PC}|NN\rangle}=\frac{\bar{M}_\Lambda}{\bar{M}_\Sigma}\left[\sqrt{\frac{8}{9}}\frac{B_\Sigma^{(3)}\langle T=1|\vec{T}_1\cdot\vec{\tau}_2|T=1\rangle}{B_\Lambda\langle T=1|\vec{\tau}_1\cdot\vec{\tau}_2|T=1\rangle}-\sqrt{\frac{1}{9}}\frac{B_\Sigma^{(1)}}{B_\Lambda}\right]=[-0.05+-0.71]=-0.76; \tag{66}$$

$$T=0:\frac{\langle\tilde{\Sigma}N|V_{\rm PV}|NN\rangle}{\langle\tilde{\Lambda}N|V_{\rm PV}|NN\rangle}=\frac{A_\Sigma^{(1)}}{A_\Lambda}=-0.56, \tag{67}$$

$$\frac{\langle\tilde{\Sigma}N|V_{\rm PC}|NN\rangle}{\langle\tilde{\Lambda}N|V_{\rm PV}|NN\rangle}=\frac{\bar{M}_\Lambda}{\bar{M}_\Sigma}\frac{B_\Sigma^{(1)}}{B_\Lambda}=2.12. \tag{68}$$

These ratios, collected in Table IV, show that the $\Sigma N\to NN$ transition is comparable with the $\Lambda N\to NN$ transition. Note that the $t=3/2$ contribution to Eq. (66) is small compared with the $t=1/2$ contribution. This is fortunate because $B_\Sigma^{(3)}$ is poorly determined (see Table III).

It is also possible to generate potentials for $\Sigma N\to NN$ transitions that proceed by means of an exchange of strange mesons (K and K^*). The connection to the related $\Lambda N\to NN$ potential is simpler in this case because the weak coupling is at the NN vertex, which is the same for each case. Only the strong ΣNK couplings are required for relating the two decay modes. Table IV shows that, unlike for the pion case, weak decays from a ΣN intermediate are always weaker than from a ΛN state when mediated by strange mesons. Furthermore, except for the spin-independent part of the K^* central potential, all the ratios in Table IV are negative. This results in a destructive interference between decays from different YN states. For K^* the spin-dependent and spin-independent components of the $T=1$ central channel interfere destructively and are delicately balanced against each other already in the $\Lambda N\to NN$ potential. Therefore, although this channel actually gets a boost from the ΣN decay mode, this can occur only because it was small (insignificantly so) to begin with.

TABLE V. Partial decay widths in units of $\Gamma_{\rm free}$, considering only the contribution of the weak π exchange. Various combinations of FFs and initial-state correlations are considered, but no final-state correlations. The "Sing" and "Dbl" entries correspond to a single FF or a FF at each vertex. The entries in the column labeled SRC are explained in the text.

FF	SRC	$S\to S$	$S\to D$	$S\to P$	Total
None	None	0.01	1.54	0.68	2.23
Sing	None	0.18	0.69	0.31	1.18
Dbl	None	0.27	1.01	0.45	1.74
Dbl	$f_{\rm HC}$	0.02	1.12	0.43	1.57
Dbl	$f_{\rm SC}$	0.11	0.96	0.39	1.46
Dbl	Tensor	0.21	1.05	0.43	1.69
Dbl	Σ	1.30	1.75	0.35	3.40

Assuming an initial S state for the ΛN pair, six matrix elements contribute to the sum in Eq. (32):

$$\begin{aligned}&T=0:{}^3S_1\to{}^3S_1,\quad {}^3S_1\to{}^3D_1,\quad {}^3S_1\to{}^1P_1;\\&T=1:{}^1S_0\to{}^1S_0;\quad {}^1S_0\to{}^3P_0;\quad {}^3S_1\to{}^3P_1.\end{aligned} \tag{69}$$

Partial widths for purely central ($S\to S$), tensor ($S\to D$), and PV ($S\to P$) decays may be defined by summation of an appropriate subset of terms. Partial widths of definite isospin may also be defined by

$$\Gamma_{\rm tot}=\frac{1}{2}\sum_T(2T+1)\Gamma_T. \tag{70}$$

These partial widths are closely related to an important observable: the ratio of the neutron-induced decay width Γ_n to the proton-induced decay width Γ_p. From Eq. (51),

$$\begin{aligned}\Gamma_n&=\Gamma_1,\\\Gamma_p&=\tfrac{1}{2}(\Gamma_0+\Gamma_1).\end{aligned} \tag{71}$$

IV. Λ DECAY WIDTH WITHOUT CORRELATIONS

A. Λ decay width: no form factor

The simplest approximation to nonmesonic Λ decay in NM involves a weak interaction incorporating only π exchange and no consideration of vertex FFs or correlations. This calculation has been performed previously by several other authors [39–41,57] as a starting point on the way to more comprehensive treatments of the nonmesonic decay. Only transitions from an initial relative S state are considered. The decay width is divided into central, tensor, and PV partial widths in Table V. For comparison, results from Ref. [40] are presented in Table VI for what is essentially the same calculation.

TABLE VI. Partial decay widths in units of $\Gamma_{\rm free}$ from Table II in Ref. [40]. These values should be compared with those in the first line of Table V.

FF	SRC	$S\to S$	$S\to D$	$S\to P$	Total
None	None	0.01	3.12	1.00	4.13

It should be noted that, in the absence of strong SRCs, the central contribution to the total decay width is sensitive to the δ-function part of the π-exchange potential. Typically it is assumed that SRCs cause the relative *YN* wave function to vanish at small distance, eliminating the δ-function contribution. As a result, it is often customary to exclude the δ-function part of the π-exchange potential *a priori* when the decay width is calculated for the unphysical case of no FF and no SRC. This custom is followed in Tables V–VII.

The evident discrepancy between the first lines of Tables V and VI is the result of a number of conspiring factors, given here in order of importance:

(1) The decay width is directly proportional to the mass of the nucleon that "catalyzes" the decay [Eq. (32)]. In Ref. [40] the free nucleon mass is used, whereas Eq. (32) employs an effective mass that is 27% smaller.
(2) A factor of $\bar{M}_Y^{-1}$ appears in the PC term of the weak π-exchange potential, Eq. (59), that is the result of a nonrelativistic reduction from a well-defined amplitude. In Ref. [40], the replacement $\bar{M}_Y \to M_N$ is made, resulting in a 20% increase in the PC partial widths.
(3) A slightly larger strong coupling constant is used in Ref. [40]: $g_{NN\pi} = 14.4$ compared with $g_{NN\pi} = 13.3$.
(4) A slightly larger weak PC coupling constant is used in Ref. [40]: $B_\pi = -7.21$ compared with $B_\pi = -7.15$.

When these differences are taken into account, the results of Tables V and VI can be reconciled to within 10%.

B. Vertex form factor

Without a FF, the π-exchange potential is singular at the origin, not merely in the central channel where there is a δ function, but in the tensor channel as well. This unphysical behavior comes from treating the *BBm* vertex as pointlike. Inclusion of a FF damps the potential smoothly at high relative momentum, effectively taking into account the internal structure and finite size of the *BBm* vertex. A standard, mathematically convenient choice for the vertex FF is a monopole form,

$$\Phi(q^2; m_\pi, \Lambda_\pi) = \frac{\Lambda_\pi^2 - m_\pi^2}{\Lambda_\pi^2 + q^2}, \tag{72}$$

with a cutoff mass, $\Lambda_\pi = 1300$ MeV, taken from the Jülich *YN* potential [30]. Following Ref. [49], a monopole FF is used at each vertex. Other authors [40,43] use a single-monopole FF for both vertices, but also a smaller cutoff mass, $\Lambda_\pi = 625$ MeV.

The FF regularization effectively broadens the δ-function component of the central potential. This yields a more diffuse interaction that will not be as sharply cut by a strong central correlation. Because the π-exchange potential is no longer singular after inclusion of a FF, contributions derived from the δ-function part of the central potential must be included. For this reason, no direct comparison for the central channel can be made between the results of Table V derived with and without a FF. Although less singular than the central potential, the tensor and PV channels are also suppressed at short range ($r < 2$ fm) by the FF.

TABLE VII. Partial decay widths in units of Γ_{free}, considering only π exchange. Various combinations of FFs and initial-state correlations are considered, but no final-state correlations. Entries are identical to those in Table V.

FF	SRC	Γ_0	Γ_1	Γ_n/Γ_p
None	None	3.77	0.23	0.11
Sing	None	1.88	0.16	0.16
Dbl	None	2.75	0.24	0.16
Dbl	f_{HC}	2.69	0.15	0.11
Dbl	f_{SC}	2.39	0.18	0.14
Dbl	Tensor	2.87	0.17	0.11
Dbl	Σ	6.36	0.15	0.05

V. EFFECTS OF STRONG CORRELATIONS ON WEAK DECAY

Strong interactions result in the ΛN pair's becoming correlated before nonmesonic decay. The situation is illustrated in Fig. 3, in which an effective weak interaction is defined when the initial ΛN pair is allowed to be correlated by the *G*-matrix effective strong interaction [32].

A. Simple correlations

The momentum-space matrix elements that determine the decay width [Eq. (32)] may be expressed in terms of wave functions for the initial and final states:

$$\langle q' J(L'S')T|V^w|qJ(LS)T\rangle = \int drr^2 \underbrace{\phi_{L'}(q'r)}_{\text{final}} \times \langle rJ(L'S')T|V^w|rJ(LS)T\rangle \underbrace{\phi_L(qr)}_{\text{initial}}. \tag{73}$$

In a typical calculation of the decay width, one accounts for correlations in the initial ΛN state by making the replacement

$$\phi_L(qr) \to \Psi_L^{JT}(qr) \equiv f_L^{JT}(r)\phi_L(qr), \tag{74}$$

where a state-dependent correlation function, $f_L^{JT}(r)$, has been introduced. As an example, Ref. [49] implements

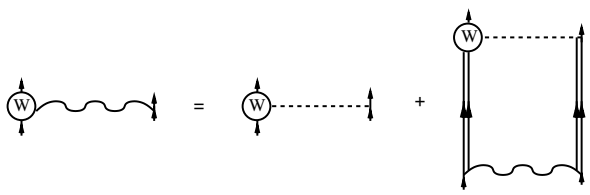

FIG. 3. Effective weak interaction incorporating strong correlations in the initial ΛN state. The wavy line represents the *G*-matrix effective interaction that properly takes into account such effects.

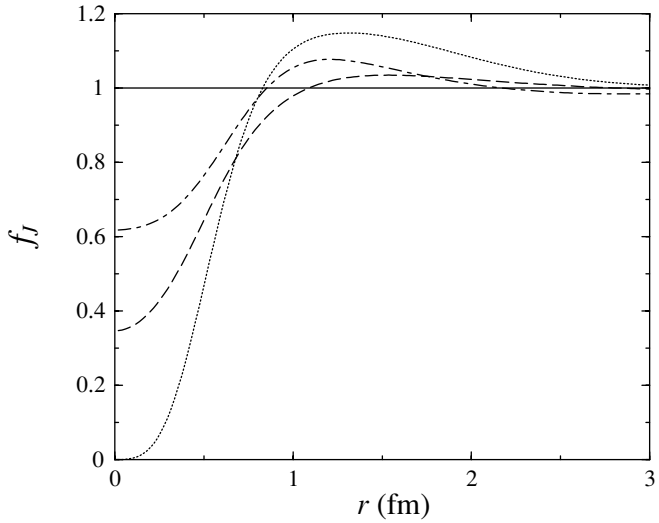

FIG. 4. Correlation functions for the $^1S_0$ (dotted-dashed curve) and $^3S_1$ (dashed curve) channels, together with the spin-independent parametrization (dotted curve) used in Ref. [49].

such a scheme to account for initial-state correlations in the nonmesonic decay of p-shell hypernuclei. A correlation function was employed that was obtained from a microscopic NM calculation [58] that utilizes the Nijmegen D hard-core potential. At least for this particular hard-core potential, a state-independent parametrization provides a good fit to correlation functions derived for either S state. Because a potential with an infinite core is used, the resultant correlation function vanishes at small distance, as can be seen in Fig. 4. The effect of this simple "hard-core" correlation function, $f_{\rm HC}$, on the decay width is presented in Table V. Correlation functions derived in a similar manner, but with the NSC potential, are also plotted in Fig. 4, and their effect on the decay width is presented in Table V under the heading $f_{\rm SC}$. The softness of the NSC potential implies weaker correlation functions and different shapes for the two S states.

The decay width can be sensitive to these modifications at small r because the weak interaction is intrinsically short range in nature. The high final-state momentum also sets a range of the order of

$$r_0 \sim \frac{\hbar c}{q_f} \approx 0.5 \text{ fm}. \tag{75}$$

The central potential is of shortest range and is expected to be most significantly affected by a correlation function. Table V shows that this is indeed the case, especially for $f_{\rm HC}$, which virtually eliminates the contribution from the central channel. However, the total decay width is dominated by the $S \to D$ transition, which is affected more modestly by the presence of a correlation function. The net result is a decrease in $\Gamma_{\rm tot}$ of 10–15% when a correlation function is used. Actually, the stronger correlation function $f_{\rm HC}$ decreases $\Gamma_{\rm tot}$ less than $f_{\rm SC}$ does. The reason for this can be seen in Fig. 4. At short range (dominantly the central channel) $f_{\rm HC}$ cuts more sharply than $f_{\rm SC}$, but at longer range (tensor channel) $f_{\rm HC}$ provides a compensating enhancement over $f_{\rm SC}$.

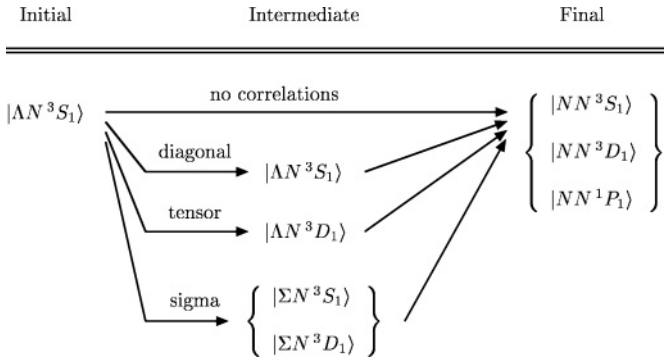

FIG. 5. Strong correlations between the ΛN pair before weak decay leads to several intermediate states from which the weak transition can subsequently proceed.

B. Beyond diagonal correlations

The treatment of correlations presented in the previous subsection is conveniently simple to implement, but incomplete and ultimately inadequate for describing nonmesonic decay. The essential problem is the coupling of channels by the strong interaction that correlates the YN system. There is a significant tensor component to the NSC89 potential that mixes angular momentum states and a strong coupling between ΛN and ΣN channels as well. A consequence of this strong coupling is the possibility of significant D-state and/or ΣN components mixed into the correlated initial ΛN S state, as illustrated schematically in Fig. 5.

For determining what fraction of the correlated ΛN S state is composed of "other" components and whether their admixture is large enough to result in a nonnegligible contribution to the nonmesonic decay parameters, an examination of the correlated wave function is required.

The effective weak interaction (Fig. 3) may be expressed in operator form as

$$V^w_{\rm eff} = V^w + V^w \frac{\Theta_{YN}}{\Omega - H_0 + i\eta} G. \tag{76}$$

When this operator acts on an uncorrelated ΛN state, $|\phi_i\rangle$, the expression

$$V^w_{\rm eff}|\phi_i\rangle = V^w|\phi_i\rangle + V^w|\phi_j\rangle \frac{\Theta_{YN}}{\Omega - E_j + i\eta}\langle\phi_j|G|\phi_i\rangle \tag{77}$$

is obtained. The repeated index indicates a sum over a complete set of YN states, $\{|\phi_j\rangle\}$, which have been inserted in the last term. The correlated state $|\Psi_i\rangle$ is naturally defined by

$$V^w_{\rm eff}|\phi_i\rangle \equiv V^w|\Psi_i\rangle, \tag{78}$$

which leads to the following expression for the correlated wave function

$$\begin{aligned} |\Psi_i\rangle &= |\phi_i\rangle + |\phi_j\rangle \frac{\Theta_{YN}}{\Omega - E_j + i\eta}\langle\phi_j|G|\phi_i\rangle \\ &\equiv (\delta_{ij} + c_{ij})|\phi_j\rangle. \end{aligned} \tag{79}$$

The implicit sum extends over all states that can couple to the initial state by means of the strong interaction. For example, if the initial state is $\Lambda N\ ^3S_1$, then the correlated state has four components, $\Lambda N\ ^3S_1$, $\Lambda N\ ^3D_1$, $\Sigma N\ ^3S_1$, and $\Sigma N\ ^3D_1$

(Fig. 5). In contrast, the simple correlation function yields a correlated wave function of the form

$$|\Psi_i\rangle = f\delta_{ij}|\phi_j\rangle, \tag{80}$$

and can account for only diagonal correlations, $i = j$, implicitly ignoring other terms that appear in Eq. (79).

A decision on which terms in Eq. (79) should be kept requires some measure by which they can be compared. It is convenient to isolate the parts of the correlated wave function that are due solely to the presense of SRC by defining the defect state

$$\begin{aligned}|\chi_i\rangle &\equiv |\Psi_i\rangle - |\phi_i\rangle \\ &= c_{ij}|\phi_j\rangle.\end{aligned} \tag{81}$$

The defect wave function has the virtue of being nonzero only in a finite range within which the strong SRCs are in effect (Figs. 6 and 7). These components of the correlated wave function are integrable and are the basis for defining a measure of the strength of correlations in each channel: the wound integral [48]. Details of the wound integral calculation are presented in the appendix.

The magnitude of the defect wave function corresponding to a given channel is not enough by itself to determine whether the channel in question will contribute significantly to the decay width. The relative strength and range of the weak potential for each channel are also critically important in determining its overall impact on the decay width.

The effective weak matrix element is related to the correlated wave function by convolution with a matrix element of the bare weak interaction. Equation (73), generalized for this case of an effective weak interaction containing a more

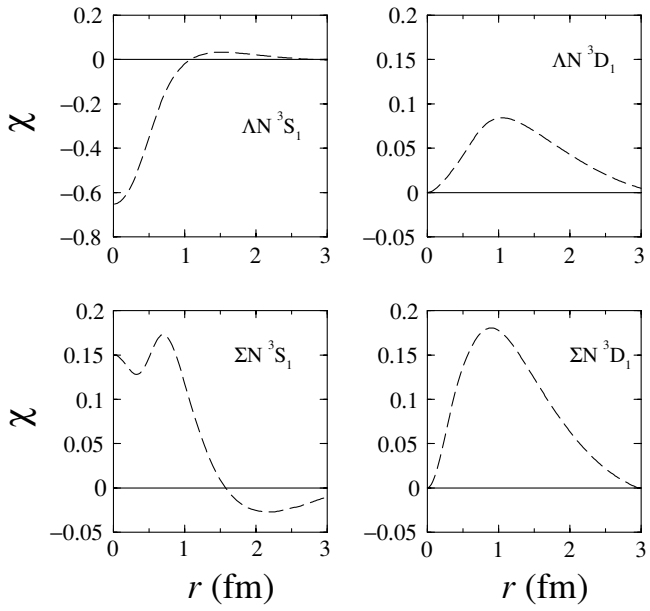

FIG. 6. Defect wave-function components of the correlated $\Lambda N\,^3S_1$ state; evaluated at the average value of the ΛN relative momentum used in Sec. II A. For comparison, the uncorrelated wave function $\phi(qr)$ is just the spherical Bessel function, $j_0(qr)$. Because of the small relative momentum, $q \sim 70$ MeV/c, $\phi(qr) \sim 0.8$ for the range shown.

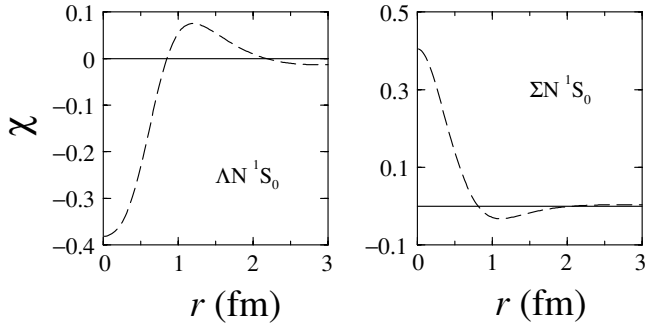

FIG. 7. Defect wave-function components of the correlated $\Lambda N\,^1S_0$ state; evaluated at the average value of the ΛN relative momentum used in Sec. II A.

intricately correlated initial state, becomes

$$\begin{aligned}&\langle q' J(L'S')T|V^{w_{\rm eff}}_{YY'}(Q,\Omega)|qJ(LS)T\rangle \\ &\quad= \sum_{L''Y''}\int dr r^2 \phi_{L'}(q'r)\langle rJ(L'S')T|V^{w}_{Y'Y''}|rJ(LS)T\rangle \\ &\qquad\times \Psi^{JTYY''}_{LL''}(qr;Q,\Omega).\end{aligned} \tag{82}$$

The π-exchange portion of the ΣN-NN transition potential is derived in Sec. III and found to be comparable with the ΛN-NN potential (Table IV). Because this is the case, the transition through the intermediate ΣN state cannot be ignored and may yield a significant contribution to both the overall decay rate and its isospin structure. The integrand of Eq. (82) is split into two pieces, the correlated initial-state wave function as one component and the balance of the integrand for the other. They are plotted together as a function of r in Figs. 8–10, one plot for each of the four possible YN states intermediate between an initial $\Lambda N\ ^3S_1$ state and final $NN\ ^3S_1, ^3D_1$ and $^1P_1$ states. The amplitudes for decay through each available intermediate state are collected in Table VIII. Also included is the amplitude for the direct decay, as would be expected from an uncorrelated state. The sum of these contributions determines the total decay amplitude for each channel.

For example, the first line of Table VIII breaks down the $^3S_1 \to {}^3S_1$ decay amplitude according to how much each portion of the correlated initial-state contributes. The first column shows the decay amplitude in the absence of any correlations. The second column indicates a large reduction that is due to diagonal correlations, as would be observed with a simple correlation function, such as those discussed in Sec. A. Likewise the first two entries in the second line show the uncorrelated decay amplitude for the direct tensor transition, $^3S_1 \to {}^3D_1$, and the small reduction caused by the diagonal SRC. The effects of these diagonal correlations are shown graphically in Figs. 8 and 9. Figure 8 illustrates the large effect a wave function depleted by correlations at short range has when paired with the very short-range central potential. Conversely, Fig. 9 indicates the poor overlap between the "hole" in the correlated wave function and the tensor potential, especially as modulated by the wave function for the final NN D state. In general, Figs. 8–10 illustrate the similarity between the range over which the defect wave function is nonzero and the range of the weak potential. This is a consequence

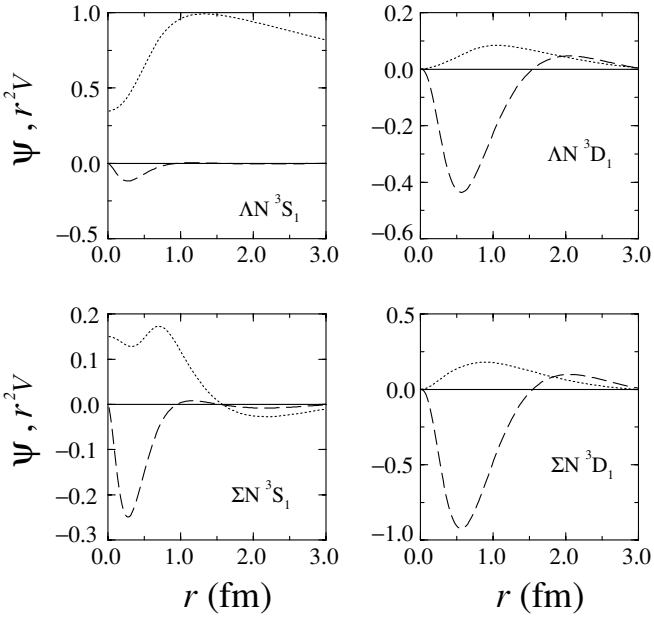

FIG. 8. Product of the weak matrix element in r space (arbitrary units) and the final-state NN wave function $\phi_0(qr)$, plotted together with correlated initial-state wave functions. $\Lambda N\ ^3S_1 \rightarrow YN\ ^3L_1 \rightarrow NN\ ^3S_1$.

of the fundamental similarities between the hypernuclear weak and strong interactions. Both share similar underlying meson-exchange structures that lead to comparable ranges. This range correspondence makes possible the significant contributions to the decay amplitude from decays proceeding through intermediate states as a result of SRCs. As a result,

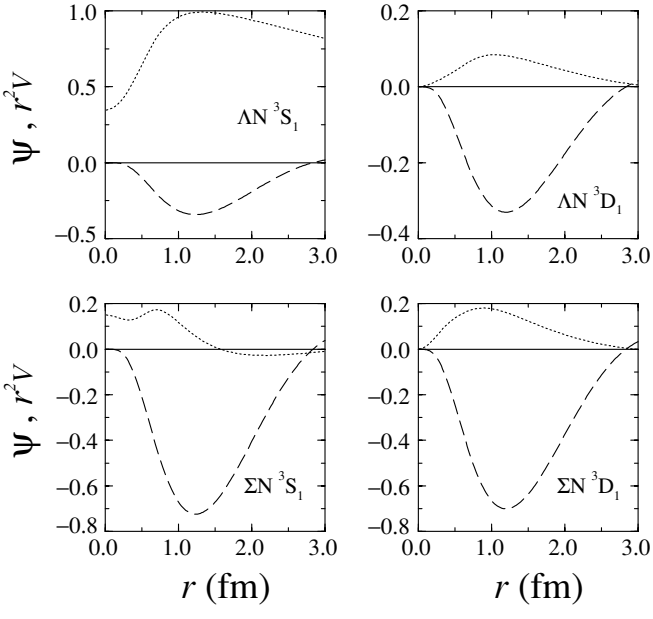

FIG. 9. Product of the weak matrix element in r space (arbitrary units) and the final-state NN wave function $\phi_2(qr)$, plotted together with correlated initial-state wave functions. $\Lambda N\ ^3S_1 \rightarrow YN\ ^3L_1 \rightarrow NN\ ^3D_1$. Weak matrix elements have been scaled up by a factor of 3 relative to $S \rightarrow S$.

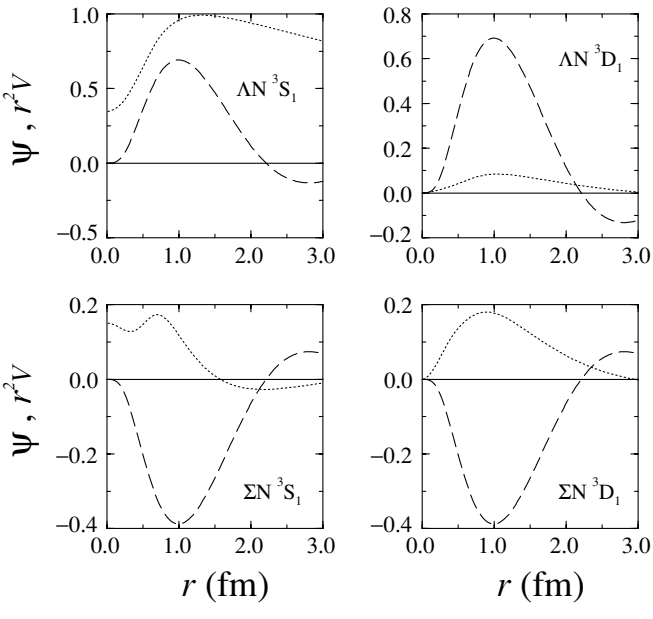

FIG. 10. Product of the weak matrix element in r space and the final-state NN wave function $\phi_1(qr)$, plotted together with correlated initial-state wave functions. $\Lambda N\ ^3S_1 \rightarrow YN\ ^3L_1 \rightarrow NN\ ^1P_1$. Weak matrix elements have been scaled up by a factor of 10 relative to $S \rightarrow S$.

at least some of the entries in Table VIII corresponding to correlation-induced transitions through intermediate YN states have magnitudes that are large enough to have a significant impact on the uncorrelated amplitudes.

The ΛN S-state column in Table VIII shows the effect of diagonal correlations on the decay amplitudes for each channel. As expected, these are substantial only for the $S \rightarrow S$ transitions to which the weak potential and final-state wave function are of shortest range. The decay amplitude in the $^3S_1 \rightarrow {}^3S_1$ channel is cut by almost 50% whereas the $^1S_0 \rightarrow {}^1S_0$ channel is cut by just under 30%. The difference is a result of the weaker correlations in the $^1S_0$ channel producing a smaller defect wave function.

The strong tensor correlations present in the ΛN system lead to a small, relatively broad, D-state component in the

TABLE VIII. Each row corresponds to one of the six possible transitions from an initial ΛN S state to a final NN state. For each channel, the matrix element for decay from an uncorrelated state is given first, and then the components of the effective weak matrix element corresponding to a transition through one of the four possible intermediate YN states, followed by the total. Matrix elements are given in units of 1.0×10^{-13} MeV^{-2}.

	No SRC	ΛNS	ΛND	ΣNS	ΣND	Total
$^3S_1 \rightarrow {}^3S_1$	−2.82	1.29	−1.35	−0.84	−4.90	−8.62
$^3S_1 \rightarrow {}^3D_1$	−7.73	0.20	−0.34	−0.93	−1.37	−10.16
$^3S_1 \rightarrow {}^1P_1$	3.65	−0.29	0.43	−0.21	−0.44	3.13
$^1S_0 \rightarrow {}^1S_0$	−2.82	0.81	0.00	0.49	0.00	−1.52
$^1S_0 \rightarrow {}^3P_0$	2.11	−0.01	0.00	−0.07	0.00	2.03
$^3S_1 \rightarrow {}^3P_1$	−1.72	0.14	0.10	0.49	−0.51	−1.50

initial-state wave function, as shown in Fig. 6. Although this piece of the correlated wave function is small, the tensor interaction coupling the intermediate D state to the final S state is considerably stronger than the corresponding central interaction. These offsetting factors combine to yield contributions to the decay amplitude of a magnitude similar to those arising from diagonal correlations but of opposite sign. The sign difference is a result of the different origin of the ΛN S-state defect wave function compared with the other pieces of the correlated wave function. Diagonal correlations serve to cut strength from the initial channel, resulting in a negative amplitude for the defect wave function, and this strength subsequently reappears in the other coupled channels, manifest as wave-function components with a positive amplitude. The result is that tensor correlations largely compensate for the reductions brought about by diagonal correlations. Of course the tensor interaction does not operate in the $J = 0$ channels, so the $^1S_0$ channel still feels the effects of the diagonal correlations.

Including decays from the ΛN relative D state leads to the "tensor" widths in Tables V and VII. Table V shows that decay widths cut by diagonal correlations are restored almost completely by tensor correlations. This is true for each of the composite channels ($S \to S$, $S \to D$, and $S \to P$) as well as the total decay width. Although diagonal correlations lower the total decay width by 15% from the uncorrelated value, inclusion of tensor correlations leaves a reduction of only 2–3%. To the extent that initial-state correlations are important at all at the level of diagonal correlations, tensor correlations will be just as important and work to counter any suppression of the decay amplitude caused by diagonal correlations. This confirms that the simple correlation function, as defined in Eq. (80), does not lead to an adequate representation of the correlated wave function. If initial-state correlations in the ΛN system are important enough to be considered, then a more general method of including correlations, Eq. (79), should be implemented.

We conclude that tensor correlations in the ΛN sector are strong enough to demand that a ΛN D-state component be included when constructing a correlated initial-state wave function. Correlations are even stronger between the initial ΛN S state and ΣN intermediate states. The ΣN components of the correlated initial-state wave function are comparable with and even slightly larger than the ΛN D-state component (Fig. 6). Furthermore, the weak transition from these ΣN intermediate states is more than twice as strong as the corresponding $\Lambda N \to NN$ decay in several channels. The result is a large amplitude for decays proceeding through the ΣN intermediates, particularly for the $T = 0$ channels in which the tensor interaction plays such a dominant role. Including decays from intermediate ΣN states leads to the "Σ" widths in Tables V and VII. The key feature to note is a *doubling* of the total decay width when Σ correlations are included. Both the $S \to S$ and $S \to D$ channels see significant increases, especially the central channel, which now rivals the tensor channel. The central channel sees such a large boost from the presence of ΣN intermediates because of the *two* tensor transitions involved in the multistep decay. Conversion to a ΣN intermediate by means of the strong tensor force is followed by a weak decay that also involves a tensor force:

$$\Lambda N\,{}^3S_1 \xrightarrow{s} \Sigma N\,{}^3D_1 \xrightarrow{w} NN\,{}^3S_1. \tag{83}$$

In contrast, the net $S \to D$ channel involves only a single tensor transition, weak or strong depending on whether the intermediate is an S state or a D state. Note that this increase comes from the $T = 0$ channels, and from Table IV the $\Sigma N \to NN$ potential has the same sign as its $\Lambda N \to NN$ counterpart. As a result, amplitudes for decays in the two $T = 0$ channels add constructively.

C. Exchange of heavy mesons

In the previous subsection, nonmesonic decay by means of virtual pion exchange was discussed. If the exchange of heavier mesons is considered, the decay properties of the Λ can be altered. To facilitate this discussion we include the coordinate-space weak-transition potentials in Figs. 11–16 for the relevant mesons. Strange mesons, in particular, are expected to contribute to a higher Γ_n/Γ_p ratio by virtue of their isospin structure. Table IX shows that the kaon by itself has a ratio of over 1 before correlations are considered and drops to only 0.65 even after correlations have taken their toll. These values lie in a range comparable with experimental values (see Sec. V E). This is in contrast to the pion-only results, which are substantially lower than both the kaon and experimental ratios, primarily because of the strong pionic tensor component. Unfortunately, hopes of bridging the gap between the pion numbers and experimental decay parameters by adding kaon decay into the mix are hampered by the relative weakness of the kaon potential. Although the $T = 1$ decay channels are comparable with the $T = 0$ channels for the kaon, resulting in a relatively large Γ_n/Γ_p ratio, they are both dominated by the $T = 0$ channels of the pion, which are

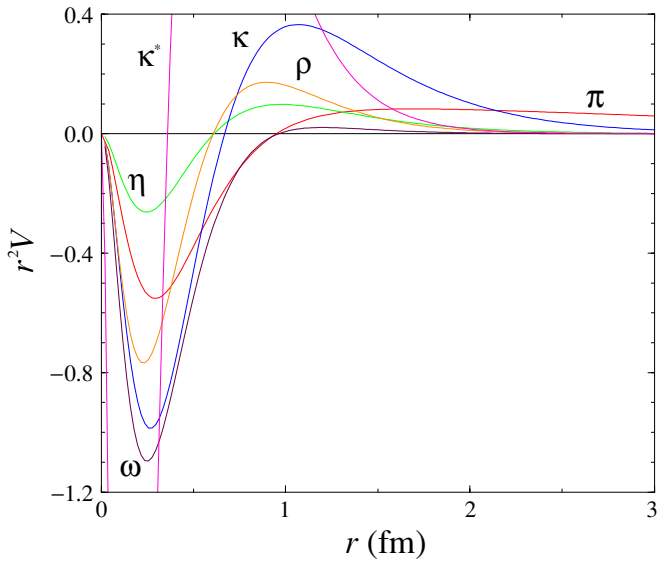

FIG. 11. (Color online) Weak potential for all mesons in the central channel in arbitrary units. The r-space potential that is due to each meson in the $^1S_0 \to {}^1S_0$ channel is shown here with the inclusion of a double-monopole FF.

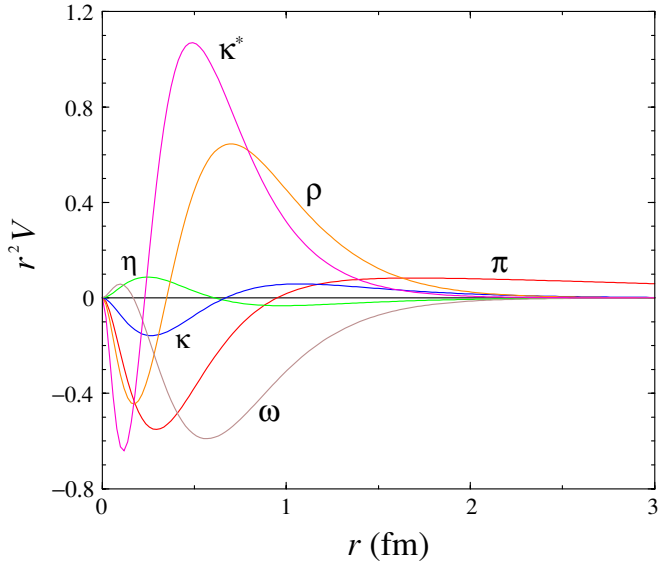

FIG. 12. (Color online) Weak potential for each meson in the central ${}^3S_1 \to {}^3S_1$ channel in arbitrary units including a double monopole.

fed by its large tensor potential. This can be clearly seen in Fig. 13, in which the pion dominates the kaon in the tensor channel, especially once convolution with the uncorrelated $l = 2$ final-state wave function is considered.

Before correlations are considered, mesons beyond the pion alter the decay widths significantly. As shown in Table X, the central $S \to S$ channels are increased the most by the new decays, raising this partial width by a factor of almost 20 from 0.27 for the pion alone to over 5.0 for the collection of mesons taken together. This strong constructive interference shows through in Fig. 11, in which the weak potentials for all mesons

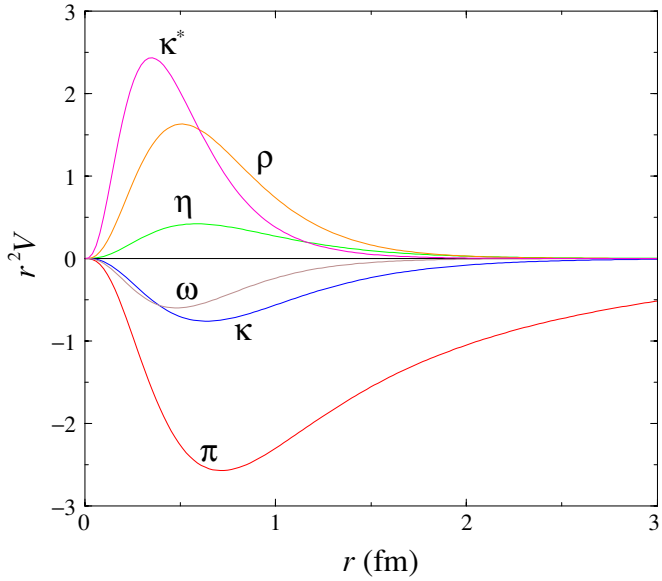

FIG. 13. (Color online) Weak potential for all mesons in the tensor channel ${}^3S_1 \to {}^3D_1$ in arbitrary units in which a double-monopole FF is used.

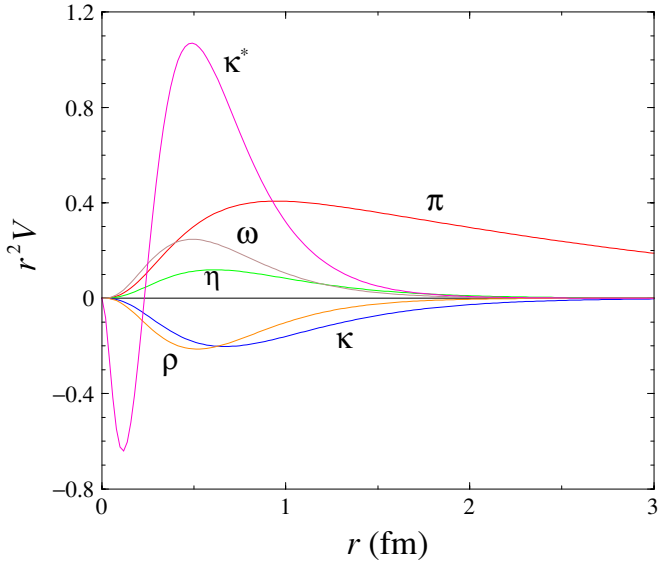

FIG. 14. (Color online) Weak potential for all mesons in the PV ${}^1S_0 \to {}^3P_0$ in arbitrary units in which a double-monopole FF is used.

in the $T = 1$ central channel are plotted. The $T = 0$ central potentials are plotted in Fig. 12, though they do not contribute significantly to the total $S \to S$ decay width. In this case, destructive interference results in a contribution to the decay width well below that of the pion alone. Many mesons have substantial decay widths in these channels, and they interfere constructively to dominate the overall decay in the absence of moderating SRCs.

Although no individual meson approaches the strength of the pionic tensor interaction, destructive interference cuts this partial width in half nonetheless (Fig. 12), likewise for the PV channels (Figs. 14–16), though here the K^* meson does possess a strength comparable with the pion. The final result is that the central channels now dominate over the tensor channel

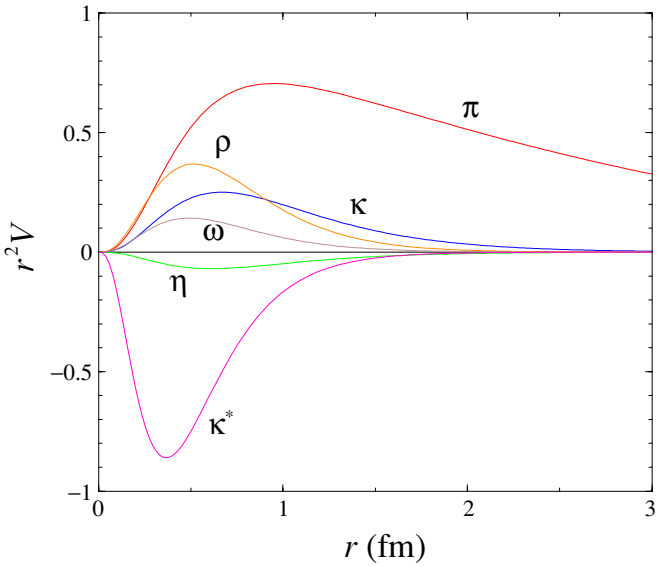

FIG. 15. (Color online) Same as Fig. 14 for the the PV ${}^3S_1 \to {}^1P_1$ transition.

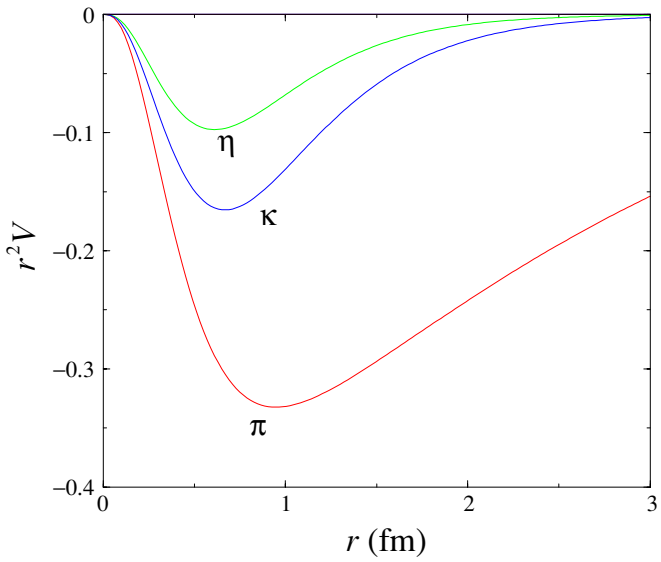

FIG. 16. (Color online) Same as Fig. 14 for the the PV ${}^3S_1 \rightarrow {}^3P_1$ transition. Only pseudoscalar mesons have nonzero potentials in this case.

and the total decay width is increased by over a factor of 4. Note that this dominance of the decay width by the central channels, specifically the $T = 1$ channel, leads to a dramatic increase in the Γ_n/Γ_p ratio. The ratio increases to 1.01, seeming to validate the inclusion of mesons beyond the pion for the purpose of reaching an agreement between experiment and theory. However, it will be seen that this agreement lasts only until initial-state correlations are considered.

Inclusion of initial-state correlations at the level of diagonal correlations changes this picture. Mesons heavier than the pion are likewise of shorter range than the pion and feel the cut of SRCs more strongly (Table XI). The result is a reduction in the partial width involving the central channels by more than a factor of 3, bringing them more in line with other contributing channels (tensor and PV). This is in contrast to the pion-only case, in which diagonal correlations cut an already small central contribution. The PV partial width is also reduced by a factor of 1/3, and the tensor width is essentially unaffected. Now the central channels are still the largest contribution,

TABLE IX. Partial decay widths in units of Γ_{free} for the pion and kaon. A double-monopole FF is used in all cases together with various choices for the initial-state correlations. No final-state correlations are included.

Mesons	SRC	Γ_0	Γ_1	Γ_n/Γ_p
π	None	2.75	0.24	0.16
π	f_{SC}	2.39	0.18	0.14
π	Tensor	2.87	0.17	0.11
π	Σ	6.36	0.15	0.05
K	None	0.11	0.14	1.12
K	f_{SC}	0.09	0.06	0.81
K	Tensor	0.11	0.06	0.68
K	Σ	0.09	0.04	0.65
$\pi + K$	Tensor	4.10	0.23	0.11

TABLE X. Partial decay widths in units of Γ_{free}, considering different meson exchanges. A double-monopole FF is used in all cases. No initial- or final-state correlations are included.

Meson	$S \rightarrow S$	$S \rightarrow D$	$S \rightarrow P$	Total
π	0.27	1.01	0.45	1.74
η	0.01	0.01	0.01	0.03
K	0.19	0.04	0.05	0.27
ρ	0.13	0.04	0.03	0.20
ω	0.58	0.01	0.01	0.60
K^*	0.48	0.03	0.21	0.72
All	5.06	0.66	1.50	7.22

and the PV (tensor) channels are still larger (smaller) than for the pion-only case. The result of diagonal correlations is a reduction of the overall width by more than half, yet still leaving it more than twice the size of the decay width for the pion alone at this level of correlation. Tensor correlations have only a modest effect, as was the case for the pion alone.

Opening the $\Sigma N \rightarrow NN$ decay channel by means of the K and K^* mesons in addition to the direct path from the ΛN initial state also has only a modest effect on the overall decay width, unlike what is observed for the pion alone. The tensor decay width is increased by almost a factor of 2, even more than in the case of the pion alone, but the width derived from the central channels actually decreases. This is in contrast to the marked increase for the pion alone, which sees the central channel rise from insignificance to rival the tensor channel when decays from the ΣN intermediate state are considered. The difference can be attributed to two things. Although the $\Sigma N \xrightarrow{\pi} NN$ decay is a very strong-decay channel that serves to increase the tensor partial width, this channel is no longer dominant, so its increase does not affect the overall width as much. The central channel also feels this particular decay channel strongly, but interference with other mesons serves to wash out its contribution, unlike for the case of the pion alone. In the end, the overall decay width sees a modest 10% increase. This in comparison with the 100% jump this new channel brings to the pion decay mode.

TABLE XI. Partial decay widths in units of Γ_{free}, considering different meson exchanges. A double-monopole FF is used in all cases together with various choices for the initial-state correlations. Note that, in the last line, decays from intermediate ΣN states are included only for those mesons for which appropriate coupling constants are available: π, K, and K^*. No final-state correlations are included.

Mesons	SRC	$S \rightarrow S$	$S \rightarrow D$	$S \rightarrow P$	Total
π	None	0.27	1.01	0.45	1.74
π	f_{SC}	0.11	0.96	0.39	1.46
π	Tensor	0.21	1.05	0.43	1.69
π	Σ	1.30	1.75	0.35	3.40
All	None	5.06	0.66	1.50	7.22
All	f_{SC}	1.51	0.68	1.10	3.29
All	Tensor	1.50	0.72	1.28	3.50
All	Σ	1.43	1.30	1.07	3.80

TABLE XII. Partial decay widths in units of Γ_{free} for the case of the full complement of mesons compared with the pion alone. Note that, for the last line, only the pion and strange mesons have ΣN decay components included. A double-monopole FF is used in all cases together with various choices for the initial-state correlations. No final-state correlations are included.

Mesons	SRC	Γ_0	Γ_1	Γ_n/Γ_p
π	None	2.75	0.24	0.16
π	f_{SC}	2.39	0.18	0.14
π	Tensor	2.87	0.17	0.11
π	Σ	6.36	0.15	0.05
All	None	2.91	0.52	0.30
All	f_{SC}	2.26	0.42	0.31
All	Tensor	2.90	0.38	0.23
All	Σ	5.20	0.49	0.17

D. Comparison: finite nuclei

Experimental results are available for medium and, to a lesser extent, heavy nuclei. Theoretical calculations have also been performed directly for finite systems, such as $^{12}_{\Lambda}$C [59], and indirectly for heavier systems by use of a local-density approximation (LDA) [60]. Collisions of protons on heavy nuclei (Au, Bi, U) have been conducted recently and yield a measure of the lifetime of heavy Λ hypernuclei [61]. This leads to a decay width of $\Gamma = 1.8$ for heavy hypernuclei. This compares with a value of close to 1 for a lighter hypernucleus such as $^{12}_{\Lambda}$C. Presumably, the total decay width measured for heavy hypernuclei should be directly comparable with a NM calculation. One caveat could be the fact that actual heavy hypernuclei have an *N*/*Z* ratio significantly larger than unity [62]. This of course depends on the Γ_n/Γ_p ratio. Another connection between the realms of high- and low-*A* hypernuclei can be forged with the aid of the LDA. This tool provides a rough but direct connection between results calculated for NM and relatively low-mass hypernuclei that are more accessible both experimentally and for direct theoretical analysis. The total decay width for a system with an average density corresponding to $^{208}_{\Lambda}$Pb is $\Gamma_{\text{tot}} = 1.59$, and for a system with a density profile approximating that of $^{12}_{\Lambda}$C, the width is $\Gamma_{\text{tot}} = 1.29$ [60]. These two considerations give a decrease in total width of something in the neighborhood of 20–45% when one compares a heavy system with a light one. This connection allows finally a comparison between the NM results of this work and LDA calculations or those performed directly for lighter finite nuclei such as $^{12}_{\Lambda}$C. Although our final-result for the total decay width is substantially larger than the experimental result in heavier nuclei or the theoretical one [60], one should keep in mind that final-state interactions have an important effect on this quantity. It is not straightforward to include these correlations in a NM calculation in a way that is relevant for the present application. It should be noted, however, that the use of dressed nucleon propagators, representing a form of NM final-state interactions (FSIs), in the intermediate state of the weak self-energy in Fig. 2, possibly interacting with each other, would lead to a substantial reduction of the imaginary part of that self-energy according to the results of Ref. [63] for the two-particle density of states. This observation confirms that such FSI effects must lead to an improved agreement with corresponding results in finite systems. A further caution concerning the comparison of NM results with those of a finite nucleus pertains to the initial-state wave function. The relative wave function between the interacting ΛN pair is different in NM compared with that in a finite system. In particular, the average Λ momentum is not zero as assumed in the NM calculations. Perhaps this increase in the average Λ momentum is washed out by the Fermi distribution of momentum of the nucleons that stimulate the nonmesonic decay. One could investigate any trend simply by varying the momentum of the decaying Λ hyperon, though this is beyond the scope of the present work. An appropriate choice of an average Fermi momentum or a more complete LDA calculation based on the present work would also be relevant in this context.

E. Γ_n/Γ_p: experiment versus theory

One of the primary observables associated with nonmesonic Λ decay is the ratio of the neutron-induced partial width $\Gamma_{\Lambda n\to nn}$ to the proton-induced partial width $\Gamma_{\Lambda p\to np}$. Theoretically the ratio has always been quite small, a value of around 0.1 typical for calculations dominated by pion exchange, as with our present NM result of 0.17 (Table XII). Theoretical results for $^{12}_{\Lambda}$C that use the same weak meson-exchange interaction are compared with experimental data in Table XIII. Recently, the long-standing discrepancy between theory and experiment concerning this ratio has begun to be resolved. Experimentally this value had been close to unity with large error bars [65,66]. Recently these error bars have been narrowed in new analyses [67–71] and smaller values of Γ_n/Γ_p have been obtained by analysis of nucleon-nucleon coincidence data including those for heavier nuclei [68,71].

The strong tensor force of the pion inevitably leads to a dominance of the $T = 0$ final states and a subsequently small Γ_n/Γ_p ratio. The $\Sigma N \to NN$ decay channel is also dominated by the tensor interaction, resulting in a further boost to Γ_p that keeps the ratio small. Likewise, uncertainty in the $\Lambda - \Sigma$ coupling strength cannot substantially alter the result if the decay is mediated by pions.

The literature contains a number of approaches to breach the gap between the older data and the results of calculations. If the $\Delta I = 1/2$ rule is violated, then it may be possible to lessen the dominance of the pion's tensor channel [72]. Direct quark models that circumvent the $\Delta I = 1/2$ rule have also been proposed [73]. In addition to purely theoretical efforts, the models and assumptions used in the experimental analyses have been examined. FSIs affect the nucleon energy distribution, and charge exchange can shift the ratio of neutrons to protons found in the final state. Uncertainty concerning the impact of these processes casts a fuzzy shadow over the quoted experimental values for Γ_n/Γ_p. It is partly due to the use of a Monte Carlo model [74] to account for FSIs that error bars on this important observable have decreased recently [67–71]. We note that the results of [67] have been superseded by those of [69] because of new results for FSI calculations [74]. Experiments now favor a value of Γ_n/Γ_p around 0.5 for $^{12}_{\Lambda}$C

TABLE XIII. Γ_n/Γ_p for different hypernuclei. Quoted theoretical results from [59] use strong coupling constants from the NSC89 interaction [29] employed in this work. The last theory entry for ${}^{12}_{\Lambda}$C lists a range of values that depends on the choice of thresholds and pair opening angles [64]. The 1*N* and 2*N* results assume values of Γ_2/Γ_{nm} around 0.3 in [67,69].

Theory/Expt.	Note	Γ_n/Γ_p	Source
Theory ${}^{12}_{\Lambda}$C	π + FSI	0.093	[59]
Theory ${}^{12}_{\Lambda}$C	$\pi + K$ + FSI	0.210	[59]
Theory ${}^{12}_{\Lambda}$C	All + FSI	0.181	[59]
Theory ${}^{12}_{\Lambda}$C	all + FSI	0.34-0.43	[64]
Expt. ${}^{12}_{\Lambda}$C		$1.33^{+1.12}_{-0.81}$	[65]
Expt. ${}^{12}_{\Lambda}$C		$1.87 \pm 0.59^{+0.32}_{-1.00}$	[66]
Expt. ${}^{12}_{\Lambda}$C	1*N*	$1.17^{+0.09+0.20}_{-0.08-0.18}$	[67]
Expt. ${}^{12}_{\Lambda}$C	1*N* and 2*N*	$0.96^{+0.10+0.22}_{-0.09-0.21}$	[67]
Expt. ${}^{12}_{\Lambda}$C	1*N*	0.51 ± 0.15(stat.)	[68]
Expt. ${}^{12}_{\Lambda}$C	1*N*	$0.87 \pm 0.09 \pm 0.21$	[69]
Expt. ${}^{12}_{\Lambda}$C	1*N* and 2*N*	$0.60^{+0.11+0.23}_{-0.09-0.21}$	[69]
Expt. ${}^{12}_{\Lambda}$C	1*N*	$0.56 \pm 0.12 \pm 0.04$	[70]
Expt. ${}^{28}_{\Lambda}$Si	1*N* and 2*N*	$0.53^{+0.13+0.25}_{-0.12-0.24}$	[69]
Expt. ${}^{28}_{\Lambda}$Si	1*N*	$0.79^{+0.13+0.25}_{-0.15-0.22}$	[69]
Expt. ${}_{\Lambda}$Fe	1*N* and 2*N*	$0.87^{+0.18+0.23}_{-0.15-0.21}$	[69]
Expt. ${}_{\Lambda}$Fe	1*N*	$1.13^{+0.18+0.23}_{-0.15-0.22}$	[69]

and appear to discount a pion-dominated decay but are much closer to theory when other mesons are included [64,75]. Still, it is important to note that because of the possible importance of two-nucleon-induced nonmesonic decays and the relevance of FSIs, no experiment can unambiguously extract the Γ_n/Γ_p ratio directly.

It is natural to look to mesons other than the pion for contributions to the nonmesonic decay that might preferentially populate $T = 1$ final states. In particular, a meson lacking a strong tensor component would be a candidate for consideration. As an example, a simple examination of the kaon coupling constants leads to an expected ratio of $\Gamma_1/\Gamma_0 \approx 40$ when only the two central channels are considered. With Eqs. (71), this leads to a Γ_n/Γ_p ratio near the maximum possible value of 2. However, this estimate implicitly assumes that the central channels dominate the kaon-mediated decay, which turns out not to be the case. Even before correlations are considered, the decay amplitude for the kaon tensor channel turns out to be comparable with the $T = 1$ central channel. With all channels taken together, including the nonnegligible PV decay channels, the Γ_1/Γ_0 ratio is sharply reduced to a value of 1.27, yielding $\Gamma_n/\Gamma_p = 1.12$. Initial-state correlations lower this value to 0.81 for diagonal correlations and further to 0.65 at the level of Σ correlations. This shows that a meson with a different potential structure from the pion can positively affect the decay observables.

It is worth pointing out that although the most recent experimental values for the Γ_n/Γ_p ratio are more precise than those obtained in the past, a certain amount of model dependence remains. In particular, it is not clear how to reinterpret these results in light of a significant contribution from Σ decays. We further note that the model dependence in the analysis is further clarified by comparing directly with nucleon-nucleon coincidence spectra [64,75] and the inclusion of FSIs between these nucleons [59], leading to better agreement between data and theory.

VI. CONCLUSIONS

The present work examines the weak-decay properties of the Λ in nuclear matter. Particular emphasis has been placed on a consistent treatment of the influence of SRCs and tensor correlations induced by the strong *YN* interaction. Such correlations allow additional pathways to contribute to the nonmesonic weak decay. In addition to the ΛN admixtures, the strong interaction also induces important ΣN components into the correlated wave function. The latter components yield nonnegligible contributions that have been substantiated by consideration of the corresponding values of their wound integrals. The present study can be summarized as follows: If initial-state correlations in the ΛN system are important enough to be considered, then a more general method of including correlations should be implemented following the method developed in this paper. A reanalysis of the weak decay of hypernuclei including such components appears therefore appropriate. The inclusion of SRCs and tensor correlations induced by the NSC89 interaction suggest that the pion-exchange mechanism still plays an important, if not dominant, role. The present work does not include the explicit consideration of FSIs that is so important in the analysis of experimental quantities. For this reason we suggest that it is not possible to draw final conclusions in comparing the present results for NM with data from finite nuclei. It is quite plausible that the inclusion of FSIs would bring the total decay width in the direction of experiment for heavier systems. For the Γ_n/Γ_p ratio we note that our value of 0.17 is still substantially smaller than the current experimental results. However, it is not clear how the data must be reinterpreted when significant contributions of Σ decays are involved. In addition, we repeat that our NM results do not include a treatment of FSIs that has a considerable influence on the value that is extracted experimentally. We finally note that other versions of realistic *YN* interactions may yield somewhat different results for weak-decay properties, as they assign different weight to the importance of the admixture of ΣN components.

ACKNOWLEDGMENTS

This work was supported by the U.S. National Science Foundation under grant no. PHY-0140316.

APPENDIX: WOUND INTEGRAL

The volume integral of the defect wave function is a measure of the combined strength and range of the strong

TABLE XIV. Wound integrals.

Channel		$\kappa^{JS}_{Y'L';YL}$	
Initial	Intermediate	NSC89	RSC
$\Lambda N\ ^1S_0$	$\Lambda N\ ^1S_0$	0.007	0.022
$\Lambda N\ ^1S_0$	$\Sigma N\ ^1S_0$	0.002	—
$\Lambda N\ ^3S_1$	$\Lambda N\ ^3S_1$	0.028	0.031
$\Lambda N\ ^3S_1$	$\Sigma N\ ^3S_1$	0.034	—
$\Lambda N\ ^3S_1$	$\Lambda N\ ^3D_1$	0.028	0.068
$\Lambda N\ ^3S_1$	$\Sigma N\ ^3D_1$	0.094	—

interaction and defines a "correlation volume":

$$V_C \equiv \sum_i \int d^3r |\langle \vec{r}|\chi_i\rangle|^2. \tag{A1}$$

The wound integral κ is defined as the ratio of V_C to the volume per particle:

$$V_0 \equiv \frac{1}{\rho} = \frac{3\pi^2}{2{k_F}^3}. \tag{A2}$$

The concept of the wound integral was introduced by Brandow [76] in the context of the Brueckner-Bethe-Goldstone theory of NM as an expansion parameter for a cluster expansion. It is tempting to argue that correlations are not important if $\kappa \ll 1$, because particles will not, on average, be within interaction range. The wound integral does provide a means of comparing the relative strength of correlations among different potentials. A "partial" κ_{ij} for each channel can be defined by

$$\kappa = \sum_{ij} \kappa_{ij} \tag{A3}$$

All of the "partial" wound integrals for an initial ΛNS state are presented in Table XIV along with values for the Reid soft core (RSC) interaction [77] for comparison. Table XIV shows that wound integrals for the NSC89 potential are of comparable size with their nuclear counterparts. These results clarify the importance of the coupling to ΣN states by the strong interaction in the weak decay of the Λ as considered in Sec. V.

[1] A. Gal, Adv. Nucl. Phys. **8**, 1 (1977).
[2] B. Povh, Annu. Rev. Nucl. Sci. **28**, 1 (1978).
[3] C. B. Dover and A. Gal, Prog. Part. Nucl. Phys. **12**, 171 (1983).
[4] T. Motoba, H. Bando, R. Wünsch, and J. Zofka, Phys. Rev. C **38**, 1322 (1988).
[5] A. A. Usmani, S. C. Pieper, and Q. N. Usmani, Phys. Rev. C **51**, 2347 (1995).
[6] D. Halderson, Phys. Rev. C **61**, 034001 (2000).
[7] M. Hjorth-Jensen, A. Polls, A. Ramos, A., and H. Müther, Nucl. Phys. **A605**, 458 (1996).
[8] I. Vidaña, A. Polls, A. Ramos, and M. Hjorth-Jensen, Nucl. Phys. **A644**, 201 (1998).
[9] J. Rożynek and J. Dabrowski, Phys. Rev. C **20**, 1612 (1979).
[10] Y. Yamamoto and H. Bandō, Prog. Theor. Phys. Suppl. **81**, 42 (1985).
[11] Y. Yamamoto and H. Bandō, Prog. Theor. Phys. **83**, 254 (1990).
[12] A. Reuber, K. Holinde, and J. Speth, Nucl. Phys. **A570**, 543 (1994).
[13] H.-J. Schulze, A. Lejeune, J. Cugnon, M. Baldo, and U. Lombardo, Phys. Lett. **B355**, 21 (1995).
[14] H.-J. Schulze, M. Baldo, U. Lombardo, J. Cugnon, and A. Lejeune, Phys. Rev. C **57**, 704 (1998).
[15] J. Dąbrowski and J. Rożynek, Prog. Theor. Phys. **105**, 923 (2001).
[16] M. Baldo, G. F. Burgio, and H.-J. Schulze, Phys. Rev. C **58**, 3688 (1998).
[17] V. G. J. Stoks and T.-S. H. Lee, Phys. Rev. C **60**, 024006 (1999).
[18] I. Vidaña, A. Polls, A. Ramos, M. Hjorth-Jensen, and V. G. J. Stoks, Phys. Rev. C **61**, 025802 (2000).
[19] M. Baldo, G. F. Burgio, and H.-J. Schulze, Phys. Rev. C **61**, 055801 (2000).
[20] I. Vidaña, A. Polls, A. Ramos, L. Engvik, and M. Hjorth-Jensen, Phys. Rev. C **62**, 035801 (2000).
[21] I. Vidaña, A. Polls, A. Ramos, and H.-J. Schulze, Phys. Rev. C **64**, 044301 (2001).
[22] A. Gal and C. B. Dover, Nucl. Phys. **A585**, 1 (1995).
[23] J. Schaffner-Bielich and A. Gal, Phys. Rev. C **62**, 034311 (2000).
[24] I. Bombaci, Phys. Rev. C **55**, 1587 (1997).
[25] M. Prakash and J. M. Lattimer, Nucl. Phys. **A639**, 433 (1998).
[26] M. M. Nagels, T. A. Rijken, and J. J. de Swart, Phys. Rev. D **12**, 744 (1975).
[27] M. M. Nagels, T. A. Rijken, and J. J. de Swart, Phys. Rev. D **15**, 2547 (1977).
[28] M. M. Nagels, T. A. Rijken, and J. J. de Swart, Phys. Rev. D **20**, 1633 (1979).
[29] P. M. M. Maessen, T. A. Rijken, and J. J. de Swart, Phys. Rev. C **40**, 2226 (1989).
[30] B. Holzenkamp, K. Holinde, and J. Speth, Nucl. Phys. **A500**, 485 (1989).
[31] T. A. Rijken, V. G. J. Stoks, and Y. Yamamoto, Phys. Rev. C **59**, 21 (1999).
[32] N. J. Robertson and W. H. Dickhoff, Phys. Rev. C **70**, 044301 (2004).
[33] E. Oset, P. Fernández de Córdoba, L. L. Salcedo, and R. Brockmann, Phys. Rep. **188**, 79 (1990).
[34] J. Cohen, Prog. Part. Nucl. Phys. **25**, 139 (1990).
[35] E. Oset and A. Ramos, Prog. Part. Nucl. Phys. **41**, 191 (1998).
[36] W. M. Alberico and G. Garbarino, Phys. Rep. **369**, 1 (2002).
[37] R. N. Silver and P. E. Sokol, editors, *Momentum Distributions* (Plenum, New York, 1989).
[38] P. Fernández de Córdoba and E. Oset, Nucl. Phys. **A528**, 736 (1991).
[39] J. B. Adams, Phys. Rev. **156**, 1611 (1967).
[40] B. H. J. McKellar and B. F. Gibson, Phys. Rev. C **30**, 322 (1984).
[41] E. Oset and L. L. Salcedo, Nucl. Phys. **A443**, 704 (1985).
[42] J. F. Dubach, G. B. Feldman, B. R. Holstein, and L. de la Torre, Ann. Phys. (NY) **249**, 146 (1996).
[43] H. Bandō, Y. Shono, and H. Takaki, J. Mod. Phys. **A3**, 1581 (1988).
[44] S. Shinmura, Nucl. Phys. **A585**, 357c (1995).
[45] A. A. Abrikosov, L. P. Gorkov, and I. E. Dzyaloshinski, *Methods*

of Quantum Field Theory in Statistical Physics (Dover, New York, 1975).
[46] A. L. Fetter and J. D. Walecka, *Quantum Theory of Many-Particle Systems* (McGraw-Hill, San Francisco, 1971).
[47] W. H. Dickhoff and D. Van Neck, *Many-Body Theory Exposed!* (World Scientific, Singapore, 2005)
[48] M. I. Haftel and F. Tabakin, Nucl. Phys. **A158**, 1 (1970).
[49] A. Parreño, A. Ramos, and C. Bennhold, Phys. Rev. C **56**, 339 (1997).
[50] J. F. Donoghue, E. Golowich, and B. R. Holstein, *Dynamics of the Standard Model* (Cambridge Univ. Press, UK, 1992).
[51] J. D. Bjorken and S. D. Drell, *Relativistic Quantum Fields* (McGraw-Hill, New York, 1965).
[52] J. J. Hernandez *et al.,* Review of Particle Properties, Phys. Lett. **B239**, 1 (1990).
[53] K. Hagiwara *et al*., Phys. Rev. D **66**, 010001 (2002).
[54] S. Gasiorowicz, *Elementary Particle Physics* (Wiley, New York, 1966).
[55] N. J. Robertson, Ph.D. dissertation, Washington University in St. Louis, 2003; available at http://wuphys.wustl.edu/ wimd/
[56] G. E. Brown and W. Weise, Phys. Rep. **22**, 279 (1975).
[57] B. F. Gibson and E. V. Hungerford III, Phys. Rep. **257**, 349 (1995).
[58] D. Halderson, Phys. Rev. C **48**, 581 (1995).
[59] A. Parreño and A. Ramos, Phys. Rev. C **65**, 015204 (2002).
[60] D. Jido, E. Oset, and J. E. Palomar, Nucl. Phys. **A694**, 525 (2001).
[61] W. Cassing *et al*., Eur. Phys. J. A **16**, 549 (2003).
[62] Z. Rudy *et al*., Eur. Phys. J. A **5**, 127 (1999).
[63] W. H. Dickhoff, C. C. Gearhart, E. P. Roth, A. Polls, and A. Ramos, Phys. Rev. C **60**, 064319 (1999).
[64] G. Garbarino, A. Parreño, and A. Ramos, Phys. Rev. C **69**, 054603 (2004).
[65] J. J. Szymanski *et al*., Phys. Rev. C **43**, 849 (1991).
[66] H. Noumi, S. Ajimura, H. Ejiri, A. Higashi, T. Kishimoto, D. R. Gill, L. Lee, A. Olin, T. Fukuda, and O. Hashimoto, Phys. Rev. C **52**, 2936 (1995).
[67] O. Hashimoto *et al*., Phys. Rev. Lett. **88**, 042503 (2002).
[68] J. H. Kim *et al*., Phys. Rev. C **68**, 065201 (2003).
[69] Y. Sato *et al*., Phys. Rev. C **71**, 025203 (2005).
[70] H. Outa *et al*., Nucl. Phys. **A754**, 157c (2005).
[71] S. Okada *et al*., Phys. Lett. **B597**, 249 (2004).
[72] A. Parreño, A. Ramos, C. Bennhold, and K. Maltman, Phys. Lett. **B435**, 1 (1998).
[73] T. Inoue, M. Oka, T. Motoba, and K. Itonaga, Nucl. Phys. **A633**, 312 (1998).
[74] A. Ramos, M. J. Vicente-Vacas, and E. Oset, Phys. Rev. C **55**, 735 (1997); **66**, 039903(E) (2002).
[75] G. Garbarino, A. Parreño, and A. Ramos, Phys. Rev. Lett. **91**, 112501 (2003).
[76] B. H. Brandow, Phys. Rev. **152**, 863 (1966).
[77] P. J. Siemens, Nucl. Phys. **A141**, 225 (1970).